1.2 A Survey of Natural Light Fields

The intricate chain of radiative transfer processes within the air and seas of the earth begins with the influx of solar radiant energy at the upper levels of the atmosphere and partially ends in the depths of the seas and lakes. We shall now briefly survey the main features of the light field in the meteorologic and hydrologic domains. We conduct the survey with the purpose of establishing the general orders of magnitudes of the set of radiometric phenomena in natural optical media which the theory of radiative transfer has been evolved to describe and predict.

The Solar Constant

The *solar (irradiance) constant* is the total irradiance produced by solar radiant energy of all wavelengths at a point located outside the earth's atmosphere at the mean distance of the earth from the sun and on a plane normal to the direction of the sun's center:

$$\text{solar (irradiance) constant} = 1396 \text{ watt/m}^2$$

$$= 2.002 \text{ gm cal/cm}^2\text{min} \qquad (1)$$

where

$$1 \text{ joule} = 0.2389 \text{ gm cal}$$

The quantity (1) is based on the results summarized by Johnson [128], and actually pertains to wavelengths in the range 220 to 7000 mμ. For a survey of solar constant measurements and some theoretical bases for them, see [296]. Table 1 gives a wavelength by wavelength analysis of the solar (irradiance) constant in watts/m^2×millimicron. In the table, $p(\lambda)$ is the percentage of the total solar constant included in the wavelength range from 0 to λ. It is interesting to note that this distribution of $H(\lambda)$ with λ is very close to the radiant emittance curve of a 6000°K complete radiator. The solar (illuminance) constant, i.e., the photometric counterpart to the solar (irradiance) constant is obtained by computing

$$E = 680\int_0^\infty H(\lambda)\ \bar{y}(\lambda)\ d\lambda \qquad (2)$$

in accordance with the general rules of photometry laid down in Sec. 1.1. We find:

$$\text{solar (illuminance) constant} = 136{,}700 \text{ lumens/m}^2 \qquad (3)$$

$$= 12{,}700 \text{ footcandles}$$

TABLE 1

Solar Spectral Irradiance Data

Wavelength in millimicrons. $H(\lambda)$ in watts/$m^2 m\mu$.

λ	$H(\lambda)$	$p(\lambda)$	λ	$H(\lambda)$	$p(\lambda)$	λ	$H(\lambda)$	$p(\lambda)$
220	0.030	0.02	420	1.92	11.7	640	1.66	42.1
225	0.042	0.03	425	1.89	12.4	650	1.62	43.3
230	0.052	0.05	430	1.78	13.0	660	1.59	44.5
235	0.054	0.07	435	1.82	13.7	670	1.55	45.6
240	0.058	0.09	440	2.03	14.4	680	1.51	46.7
245	0.064	0.11	445	2.15	15.1	690	1.48	47.8
250	0.064	0.13	450	2.20	15.9	700	1.44	48.8
255	0.10	0.16	455	2.19	16.7	710	1.41	49.8
260	0.13	0.20	460	2.16	17.5	720	1.37	50.8
265	0.20	0.27	465	2.15	18.2	730	1.34	51.8
270	0.25	0.34	470	2.17	19.0	740	1.30	52.7
275	0.22	0.43	475	2.20	19.8	750	1.27	53.7
280	0.24	0.51	480	2.16	20.6	800	1.127	57.9
285	0.34	0.62	485	2.03	21.3	850	1.003	61.7
290	0.52	0.77	490	1.99	22.0	900	8.95	65.1
295	0.63	0.98	495	2.04	22.8	950	0.803	68.1
300	0.61	1.23	500	1.98	23.5	1000	0.725	70.9
305	0.67	1.43	505	1.97	24.2	1100	0.606	75.7
310	0.76	1.69	510	1.96	24.9	1200	0.501	79.6
315	0.82	1.97	515	1.89	25.6	1300	0.406	82.9
320	0.85	2.26	520	1.87	26.3	1400	0.328	85.5
325	1.02	2.60	525	1.92	26.9	1500	0.267	87.6
330	1.15	3.02	530	1.95	27.6	1600	0.220	89.4
335	1.11	3.40	535	1.97	28.3	1700	0.182	90.83
340	1.11	3.80	540	1.98	29.0	1800	0.152	92.03
345	1.17	4.21	545	1.98	29.8	1900	0.1274	93.02
350	1.18	4.63	550	1.95	30.5	2000	0.1079	93.87
355	1.16	5.04	555	1.92	31.2	2100	0.0917	94.58
360	1.16	5.47	560	1.90	31.8	2200	0.0785	95.20
365	1.29	5.89	565	1.89	32.5	2300	0.0676	95.71
370	1.33	6.36	570	1.87	33.2	2400	0.0585	96.18
375	1.32	6.84	575	1.87	33.9	2500	0.0509	96.57
380	1.23	7.29	580	1.87	34.5	2600	0.0445	96.90
385	1.15	7.72	585	1.85	35.2	2700	0.0390	97.21
390	1.12	8.13	590	1.84	35.9	2800	0.0343	97.47
395	1.20	8.54	595	1.83	36.5	2900	0.0303	97.72
400	1.54	9.03	600	1.81	37.2	3000	0.0268	97.90
405	1.88	9.65	610	1.77	38.4	3100	0.0230	98.08
410	1.94	10.3	620	1.74	39.7	3200	0.0214	98.24
415	1.92	11.0	630	1.70	40.9	3300	0.0191	98.39

TABLE 1 (Continued)

λ	H(λ)	p(λ)	λ	H(λ)	p(λ)	λ	H(λ)	p(λ)
3400	0.0171	98.52	4400	0.0067	99.29	4900	0.0044	99.48
3500	0.0153	98.63	4500	0.0061	99.33	5000	0.0042	99.51
3600	0.0139	98.74	4600	0.0056	99.38	6000	0.0021	99.74
3700	0.0125	98.83	4700	0.0051	99.41	7000	0.0012	99.86
3800	0.0114	98.91	4800	0.0048	99.45			
3900	0.0103	98.99						
4000	0.0095	99.05						
4100	0.0087	99.13						
4200	0.0080	99.18						
4300	0.0073	99.23						

(From [128], by permission)

By dividing the solar constant by the approximate solid angle subtense of the sun at the mean distance of earth from sun, $\Omega = 6.8 \times 10^{-5}$ steradians, we obtain the approximate solar radiance and luminance constants:

$$N = 2 \times 10^{7} \text{ watts/m}^2\text{sr}$$
$$B = 2 \times 10^{9} \text{ lumens/m}^2\text{sr} \qquad (3a)$$

General Irradiance Levels at Earth's Surface

The irradiance levels at the earth's surface can vary relatively widely because of correspondingly wide variations of atmospheric clarity and elevation differences of locales above mean sea level. Hence the magnitudes to be offered here are not as unique or invariable as the solar constant given above, and must be understood as general indicators of typical irradiance levels at the earth's surface. Table 2 is adapted from one given by Moon [185]. The solar constant values in the indicated ranges have been computed from Table 1 above and included for comparison. The column marked "405 to 704 mμ" is of especial interest since it gives the irradiances in the visible portion of the spectrum. By an odd numerical fluke, the solar irradiance constant 555 watts/m^2 over the visible spectrum numerically equals the wavelength (in mμ) at which the photopic luminosity curve has its maximum. It is instructive to study the tabulated effects of moisture content of the air and altitude on the irradiance as given in Table 2. (The totals have been rounded out so as not to appear misleadingly accurate.) Quite a battery of empirical models have been evolved to predict the effects of moisture, dust, elevation of sun and of observer on the measured irradiances on the earth's surface. An excellent summary of these models may be found in [96]. Another reference, of interest to oceanographers, would be [173]. For a recent survey of solar irradiation measurements, see [296].

TABLE 2

Irradiance Data at Earth's Surface

(in watts/m^2 on a plane normal to sun's rays, within indicated portions of the electromagnetic spectrum)

Conditions	Wavelength Range				
	Below 346 mμ	346 to 405 mμ	405 to 704 mμ	Above 704 mμ	Total
Mountain tops, sun at zenith, dry clean air.	23	47	484	668	1220
Mountain tops, sun at zenith, moist dusty air.	16	43	466	534	1060
At sea level, sun at zenith, dry clean air.	16	42	472	665	1200
At sea level, sun at zenith, moist dusty air.	4	30	375	425	834
Solar (irradiance) Constant (for comparison)	58	76	555	707	1396

(From [185], by permission)

General Illuminance Levels at Earth's Surface

An extensive photometric survey of illuminance at sea level on a horizontal plane under various sky conditions was made by Brown [35], part of which is summarized in Fig. 1.12. The graphs in Fig. 1.12 give a detailed photometric portrait of the extremes of variation and the modes of variation of natural illumination generated by the light from the sun and the moon. We have seen in (3) that the solar (illuminance) constant is 12,700 footcandles, which corresponds to a solar disk luminance of 2×10^9 blondels. This level of illumination is approached by the "unobscured sun" curve in Fig. 1.12 for zenith sun. Notice how little the average overcast conditions affect the general order of magnitude of the sea level illuminance. Inexperienced bathers who think they will be safe from sunburn under overcast skies will do well to take note of this fact which follows from Fig. 1.12: one can get baked just as severely under overcast skies as in bright direct sunlight. Moonlight bathing is harmless--photometrically speaking--for, the average level of full moonlight illuminance

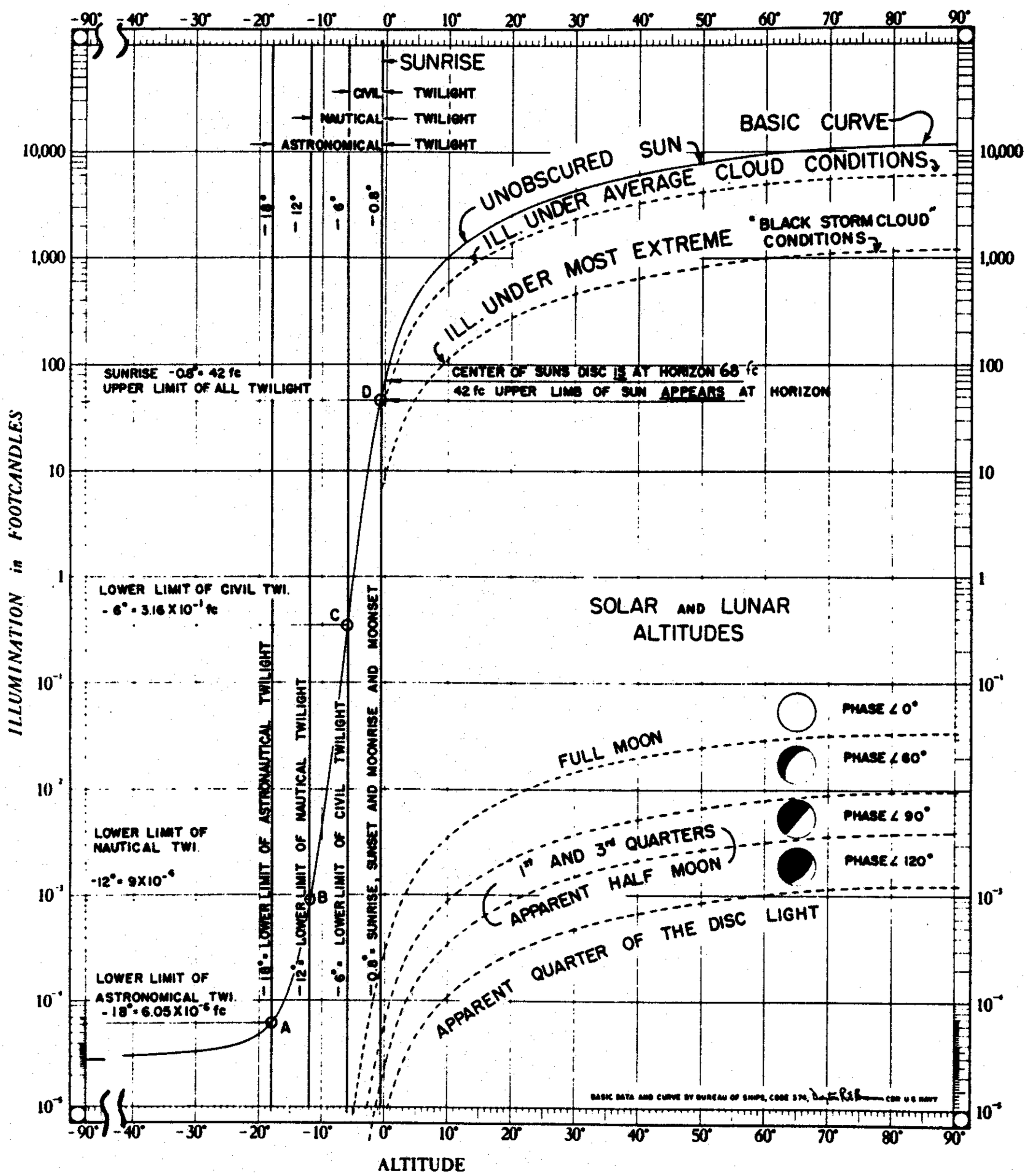

FIG. 1.12 Illuminances on a horizontal surface at sea level under indicated conditions. (From [35], by permission)

is about five orders of magnitude less than corresponding sunlight conditions. Typical clear sky luminances away from the sun are on the order of 3000 blondels, with very heavily overcast skies on the order of 300 to 1000 blondels at the zenith. For further details on the use of the graph in Fig. 1.12, one should consult the discussion given in [35].

Gross Features of Atmospheric Radiative Transfer

The tables and graphs of the irradiance and illuminance surveyed above show the great temporal and spatial variations possible in the magnitudes of these quantities. Therefore to try to assign specific numbers to the reflectance and transmittance of the atmosphere at any given time is seldom an instructive activity. However, discernable patterns and stable percentages emerge when the daily variations of the reflectances and transmittances are averaged over long times and over great areas. Such averages begin to show the general features of the radiative transfer processes extant in the atmosphere, and help us form an initial picture of the radiant energy budget of the atmosphere-surface system. Consider, for example, the average yearly irradiance (of all wavelengths) on an average horizontal surface just outside the atmosphere over the entire northern hemisphere. On purely geometrical grounds, this amounts to about one quarter of the solar constant or 340 watts/m^2 (about 0.485 gm cal/cm^2 min) over one year.

The annual radiant energy budget may be analyzed as follows: for easy visualization, we normalize the 340 watts/m^2 and start with 100 watts/m^2. Thus, if 100 units of irradiance on the average are incident on the upper atmosphere, then the general radiative transfer activities in the atmosphere at steady state are reflection, absorption, and transmission, which take up, respectively, 34, 19, and 47 of these 100 incoming units as shown in (a) of Fig. 1.13. Part (b) of Fig. 1.13 breaks the reflected and transmitted fluxes down even further. Thus, of the 34 units reflected, 25 of these are by the clouds, and 9 by the clear atmosphere. Of the 47 units transmitted, 24 of these are directly transmitted (without scattering), and 23 are transmitted via scattering. Of these 23 transmitted units 17 are transmitted by the clouds, and 6 by the clear atmosphere.

Now the 47 transmitted units are received in turn by the earth (terra firma + terra infirma), are chewed up and are eventually given back via heat radiation (14 units), or latent heat of evaporation in cloud formation (23 units) or via convection-conduction activity between the atmosphere and the earth's surface (10 units). This is shown in (c) of Fig. 1.13.

An exact mathematical formulation of these interactions can be written down using the principles of invariance for irradiance, as described generally in Sec. 8.7, assuming, e.g., a three-layer system (atmosphere + clouds + earth's surface); see in particular Examples 5 and 6 of Sec. 8.7. The numbers cited above, however, are not theoretical, but rather based on actual observations and are patterned after the

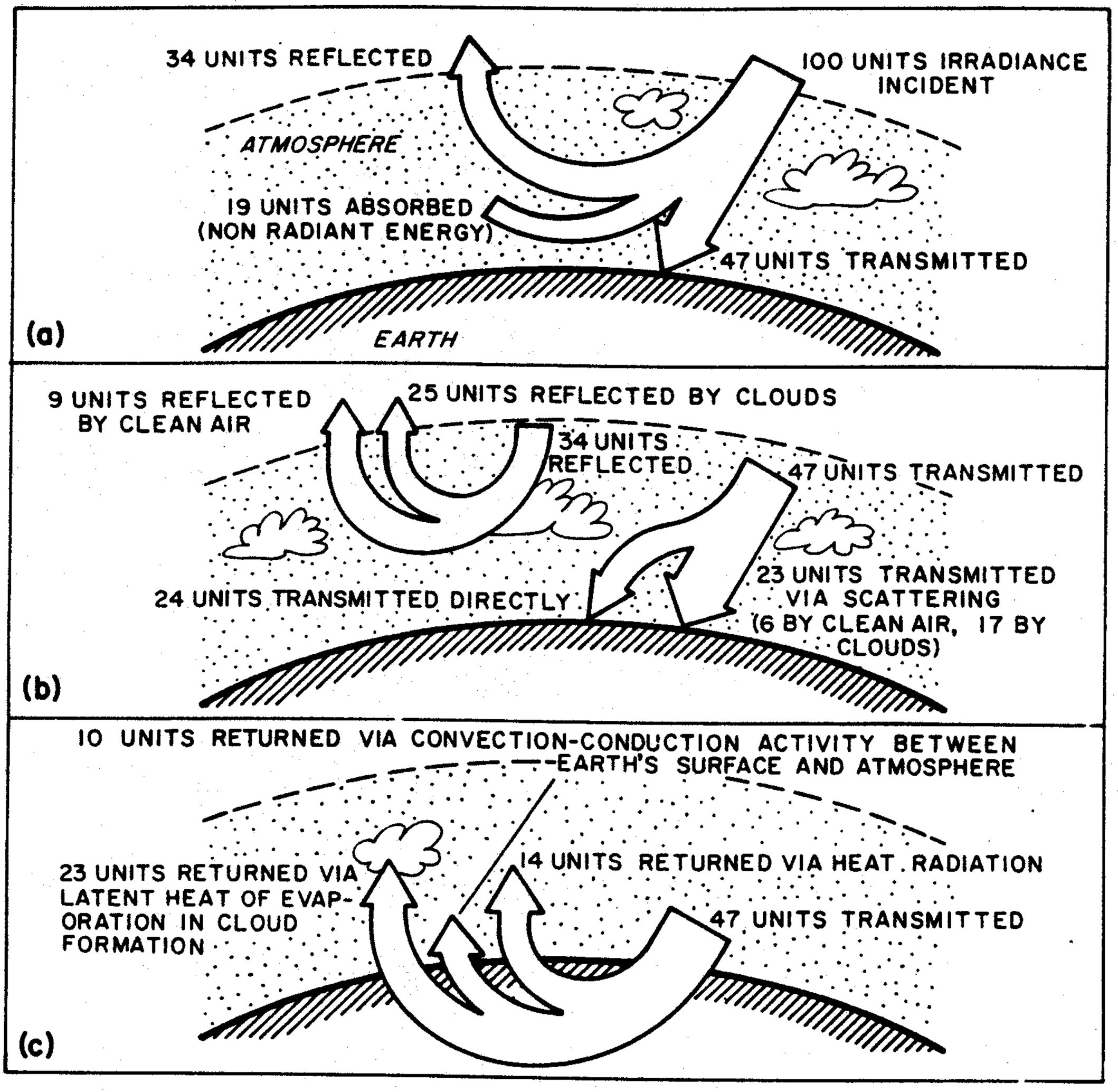

FIG. 1.13 The average yearly radiant flux budget over the sunlit hemisphere of earth. (From [96], by permission)

magnitudes summarized in [96].

Radiative Transfer Across the Air-Water Surface

The still air-water surface acts like an imperfect mirror which reflects only about 2% of an unpolarized light beam normally incident on it from the air side, and transmits about 98% of the incident flux of the beam into the water below. As the beam is tipped and all other factors the same, this reflectance stays fairly constant until, at about 45° from the vertical, the reflectance curve begins to soar to a complete reflectance of unity at grazing incidence to the air-water surface. The functional dependence of this reflectance is quite well known and is governed by Fresnel's formulas, to be studied in Sec. 12.1.

When the air-water surface is ruffled by capillary waves induced by the wind, or when the surface is heaving with gravity waves, the average amount of flux reflected from a vertical light beam incident on the moving surface over a given time can be computed, once again by means of the Fresnel reflectance function, but now with that function's values weighted by numbers between 0 and 1 which are the fraction of the given time interval the surface is tipped away from the horizontal by a given angle between 0 and 90°. The determination of these weighting factors required in such a computation is at present principally an empirical matter, and one of the first such determinations made in hydrologic optics is depicted in Fig. 1.14. This curve, based on the experimental researches by Duntley in [82], gives the number of times the water surface normal at a fixed point was observed to tip over by an amount ϕ, $0° \leq \phi \leq 90°$, during a given time period. The solid curve is for the case where the normal was observed within the up-down wind plane; the dashed curve is for the cross-wind plane case. There is very little difference between the two cases. A steady wind of 18 knots (about 9 m/sec) was blowing and maintaining a steady capillary wave and small gravity wave complex. It was found that the number n_ϕ of times the wave surface normal was tipped $\phi°$ from the vertical, during the experiment was very nearly expressible as:

$$n_\phi = n_o \, e^{-\frac{\tan^2 \phi}{2\sigma^2}} \tag{4}$$

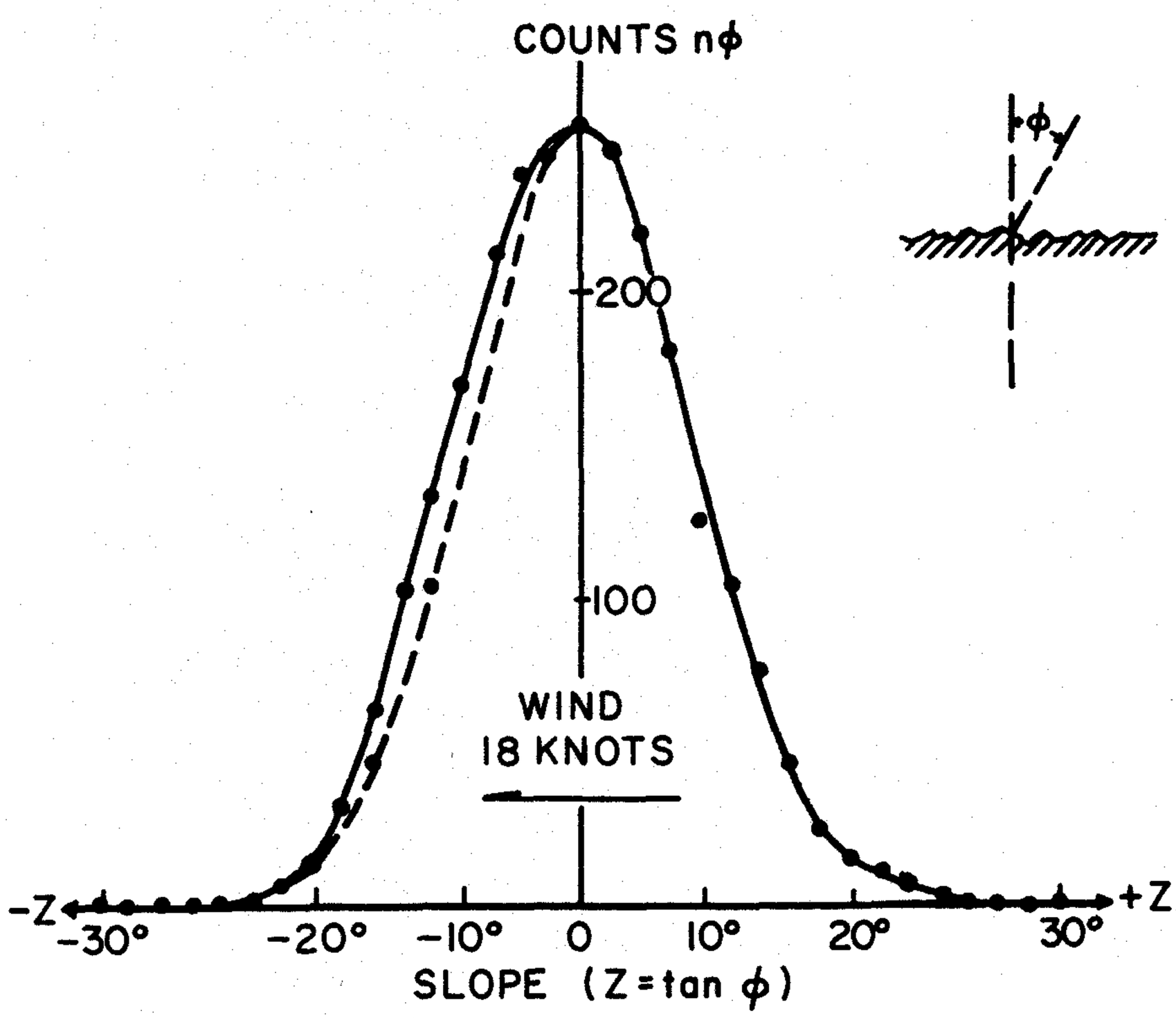

FIG. 1.14 Relative frequency of occurrence of a given tilt of a water wave facet.

In other words, n_ϕ was found to vary in a gaussian manner when tan ϕ (rather than ϕ) was used as an independent variable. The quantity σ is the usual standard deviation of the observed slopes (the mean slope tan ϕ was zero). It is clear then, that the relative number of times the wave *slopes* were tipped at tan ϕ, is given by n_ϕ/n_o. For the 18 knot wind, it turned out that σ was 0.162, which may be pictured as the tangent of a standard deviation angle of inclination of the surface normal of about 9.2 degrees from the vertical. It was also found that the square of σ, i.e., σ^2, varied nearly linearly with the surface wind speed generating and sustaining the steady wave complex. A flat calm surface clearly has a σ of 0. The preceding gaussian distribution was also found by Cox and Munk [56] in their study of the glitter patterns on the sea surface.

The preceding statistical type of description of the dynamic air-water surface can be used, under suitable conditions, to estimate the time averaged reflectance and transmittance of the air-water surface over a given time interval at a certain point; or dually, to estimate the space averaged reflectance and transmittance of the surface over a given region at a certain time instant. Table 3 displays three reflectances computed under the indicated conditions.

TABLE 3

Irradiance Reflectance H(0,+)/H(0,-) of the Air-Water Surface for Sky Light

Sky	Air-Water Surface	
	Smooth (σ=0)	Rough (σ=0.2)
Clear, sun at 60° from zenith	(no wind) .100	(13-18 knot wind) .071-.088
Uniform	.066	.050-.055
Overcast	.052	.043-.044

(From [58], by permission)

Thus under a clear sky with the sun at 60° from the zenith, a smooth sea surface will reflect about 10% of its total irradiance (H(0,-)) back into the sky, whereas, under the same sky condition, a sea driven by a steady 13-18 knot wind would reflect a slightly less amount of about 7 to 9% of the total irradiance (over the whole spectrum). This is in reasonable accordance with an intuitive estimate based on the Fresnel reflectance function for the air-water surface. In all displayed cases in Table 3, the irradiance reflectance decreases when the wind starts to blow over the surface and hence roughens the surface. As Cox and Munk observe, this fact has an important oceanographic significance, namely that in summer the open stretches of the Arctic Ocean surface (or any

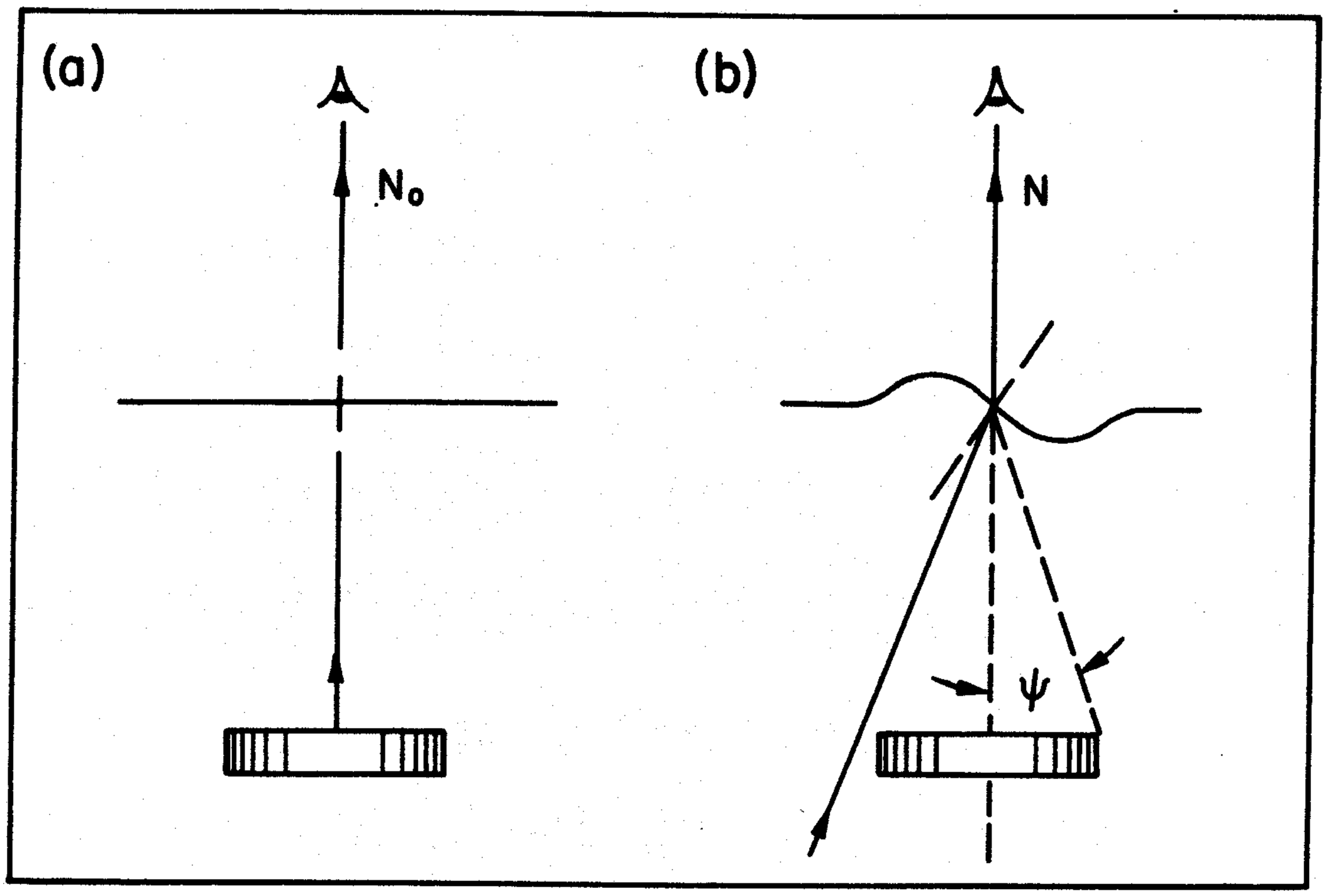

FIG. 1.15 Contrast reduction by time-averaged refraction at the air-water surface.

roughened surface for that matter) will reflect less and transmit more radiant flux than has been previously estimated using simple unweighted Fresnel reflectances (cf. [58]). More exact values of the reflectance for $\sigma = 0$ are given in Table 4 of Sec. 12.1.

A complete theory of the reflectance and transmittance of both the static and dynamic air-water surface is developed in Chapter 12 below.

Besides oceanographic applications there are also visibility applications of the observed gaussian structure of the ruffled air-water surface slopes. Thus while it is commonplace that the visibility of a submerged object below a wind blown surface as seen through the surface is less than when the surface is calm, due to the blurring action of the refracting processes at the surface, it is possible actually to make quantitative predictions of the time-averaged apparent contrast of a given submerged object against its background as a function of the size of the object and the standard deviation σ of the wave slopes through which the line of sight is directed. Part (a) of Fig. 1.15 depicts the basis of such predictions when the surface is flat and horizontal at the point of intersection with the line of sight, and when the center of the submerged object (here a circular disk) is observed to have an apparent radiance N_o. When the surface is tipped, as in (b) of the figure, the refracted line of sight picks up the apparent radiance N of the background of the object. The still water apparent contrast C of the center of

the object with respect to its water background is by definition $(N_o-N)/N$. If the time-averaged apparent contrast of the object against its background is $\overline{C}$ when the surface slopes have a standard deviation of σ, then it can be shown that:

$$\overline{C} = C\left(1-e^{-\frac{\tan^2\psi}{2\sigma^2}}\right), \tag{5}$$

where the object has an angular radius of ψ. Observe that for $C > 0$, if σ increases, then $\overline{C}$ decreases for a given ψ, as would be expected. Further, for given σ, the time-averaged contrast $\overline{C}$ increases as ψ increases; again as would be expected, but now in a definite quantitative way. For small objects or rough seas (or both) the preceding formula yields the rule of thumb:

$$\overline{C} = C\left(\frac{\tan^2\psi}{2\sigma^2}\right) . \tag{6}$$

These formulas, which describe the contrast reduction by time-varying refraction effects, will be developed in detail in Sec. 12.14.

Glitter Patterns on the Air-Water Surface

Sunlight reflected from a still air-water surface can be seen, by each observer, as a circular image lying angularly just as far below the observer's horizon as the sun lies above that horizon. A slight breeze disturbs the water and the single image splits into two or more irregularly shaped randomly moving images of the sun. The breeze continues and the few images ignite into a dazzling glitter pattern. To a poetically inclined observer, the glitter pattern invokes very ungeometrical and unhydrodynamical thoughts. In Russian, for example, the glitter pattern is sometimes referred to as the "road to happiness". However, to analytically inclined observers, the glitter pattern contains a wealth of information about the geometrical structure of the surface, the statistical distribution of wave slopes and, as we have seen above, important consequences for the radiative transfer processes across the air-water surface.

As an illustration of these more technical ideas consider the problem of finding the greatest occurring slopes on a rough sea surface at a given time. It is seemingly impossible to do this visually or even with photographs or other optical means until certain geometrical features of the sun's glitter pattern come under scrutiny. Then it becomes clear that in order for an observer to see the instantaneous reflected image of the sun in a wave facet, the three participants in this phenomenon, namely the sun, the facet, and the observer, must subtend very precise geometrical relations. These relations are readily calculated using a bit of analytic geometry. Figure 1.16 (adapted from Minnaert [182], in turn

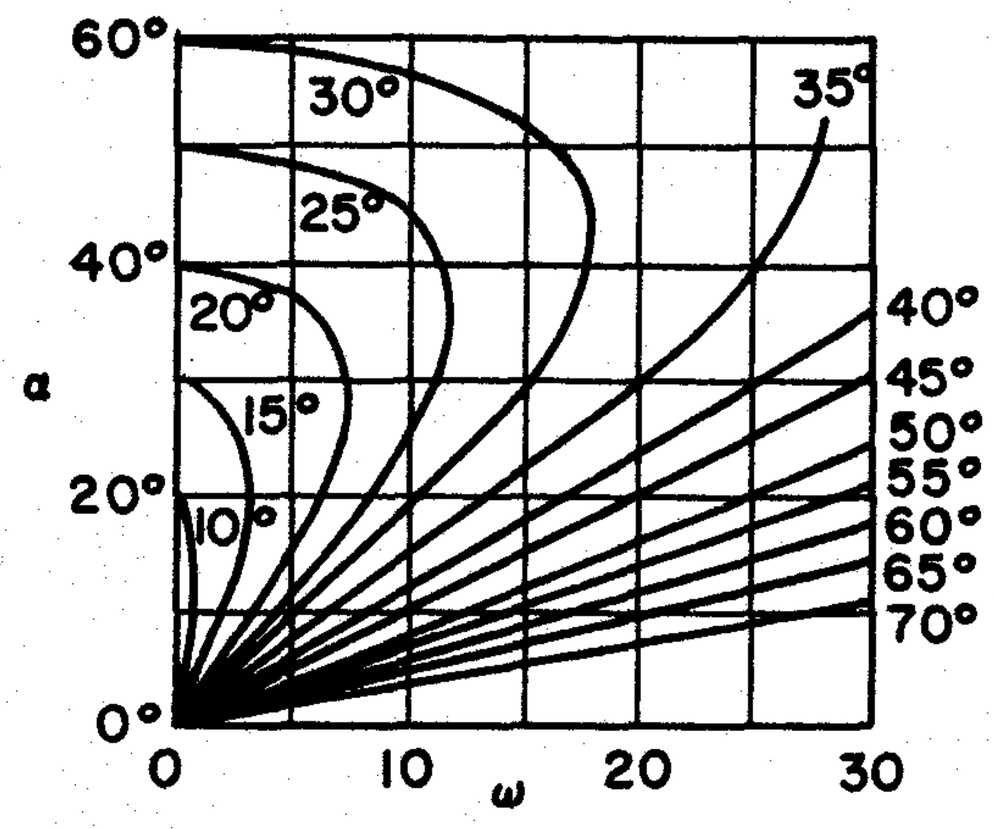

FIG. 1.16 How to find the tilt of a sun-reflecting water facet's normal knowing the sun altitude α and the horizontal angle ω of the facet from the vertical plane containing the sun. (Based on Hulburt's calculation) (From [113], by permission)

derived from [113]) summarizes one such calculation, and may be used as follows to estimate the required maximum tilt of wave facet-normals on an air-water surface which has a glitter pattern. First estimate the angular half-width ω of the pattern, and estimate the altitude α of the sun above the horizon. Suppose, e.g., ω = 15° and α = 30°. Then the curve going through the grid point (15°, 30°) is labeled "30°" and this is the requisite maximum tilt of the normals to the glittering facets. When a grid point (such as (20°, 40°)) falls between two curves, one must visually interpolate to find the requisite maximum tilt (about 32° in this case). These and related calculations are studied further in Sec. 12.5.

It is of interest to observe that the graphs in Figure 1.16 may be used to estimate the amount of tilt of *any* observed reflecting air-water facet; furthermore the object reflected in the facet need not be the sun--any point source whose distance from the facet is several times greater than the observer-facet distance may replace the sun.

Subsurface Refractive Phenomena

Once one descends below the air-water surface a new realm of relatively strange radiative transfer phenomena is encountered. At the very instant light passes that incredibly thin air-water film the radiance function receives a jolt in the form of an abrupt increase in radiance of the sky in each observable direction. The increase is by a factor of $(4/3)^2$ or 16/9. This is a purely geometric effect due to the

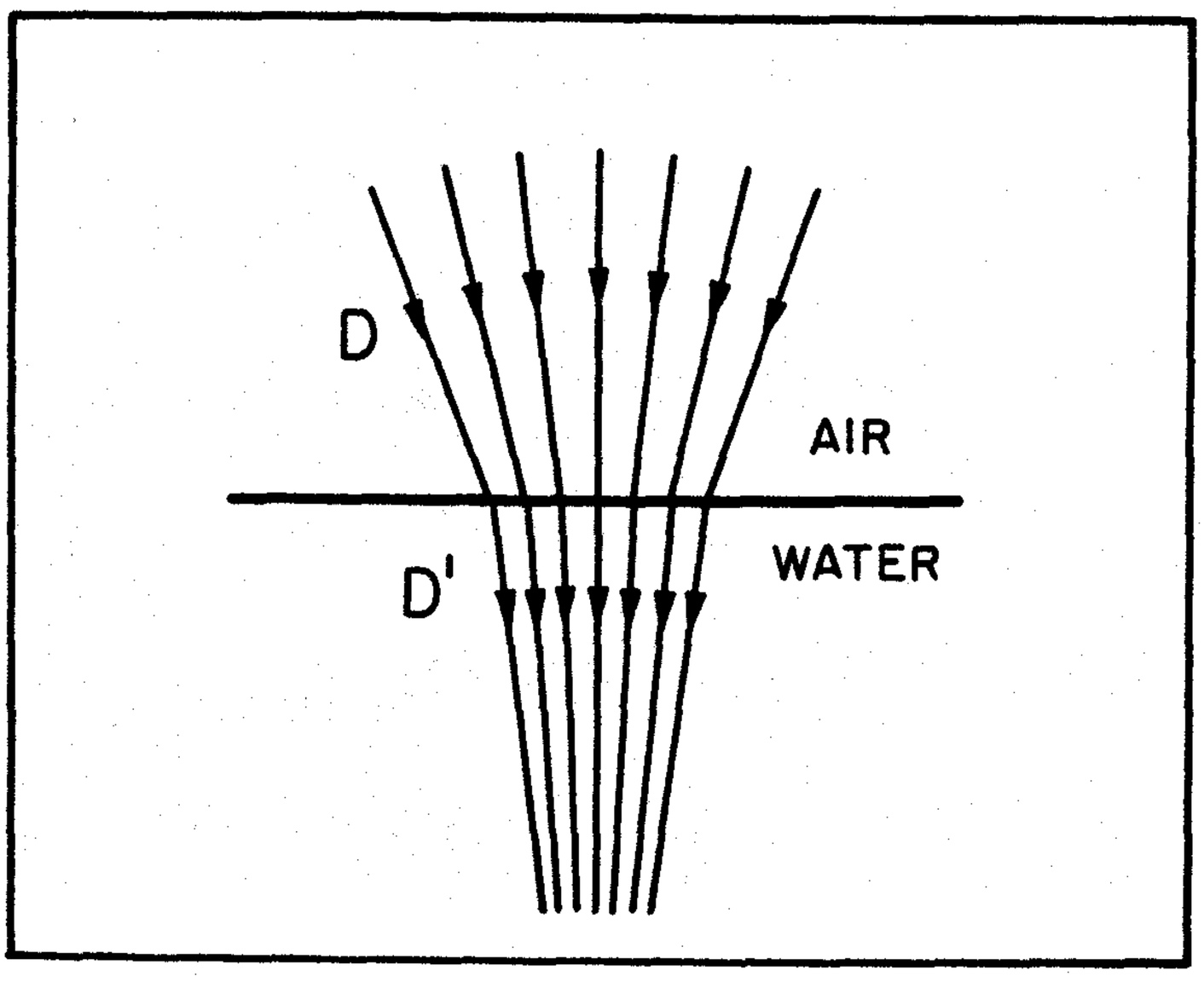

FIG. 1.17 The effect which gives rise to the n^2-law for radiance.

general narrowing of a bundle of refracted light rays as they enter the more dense water from the air (see Fig. 1.17). It is interesting to note that this phenomenon, as such, is not detectable by the unaided eye since the apparent radiance associated with a bundle of light rays depends (scattering effects aside) only on the indices of refraction at the beginning and end of the light bundle's path. Since the bundle begins in air and ends on the retina *inside* the eye, the intermediate water domain has no effect in this special geometrical sense. The full effect, however, can be measured by simple radiance meters, if they are suitably built.

The optical distortions attendant upon the refraction of the light rays at the surface are quite marked. For example as one slowly descends into a body of water with a relatively calm surface and continues to look upward, one is struck with the impression that he has just descended downward into a room with a circular hole--a "manhole"--in its ceiling. Through this manhole one sees the objects above the surface become visually compressed the closer their images lie to the rim of the hole (Fig. 1.18). Just to one side of the hole the underside of the air-water surface appears as a slightly undulating perfect mirror, in which nearby fish or other objects may be imaged--upside down. Also, if the bottom is just below the observer, he can see it mirrored on the surface above him around the rim of the manhole. As one descends further the manhole's outline is slightly dimmed by the scattering and absorbing effects of the water, but it continues to subtend the same angular radius--about 48°, the angle beyond which, according to Snell's law of refraction, total internal reflection takes place.

If the air-water surface is not calm, but ruffled with wavelets, then the ideal geometric reflection pattern is replaced by something relatively complex. Beebe [12] gives the

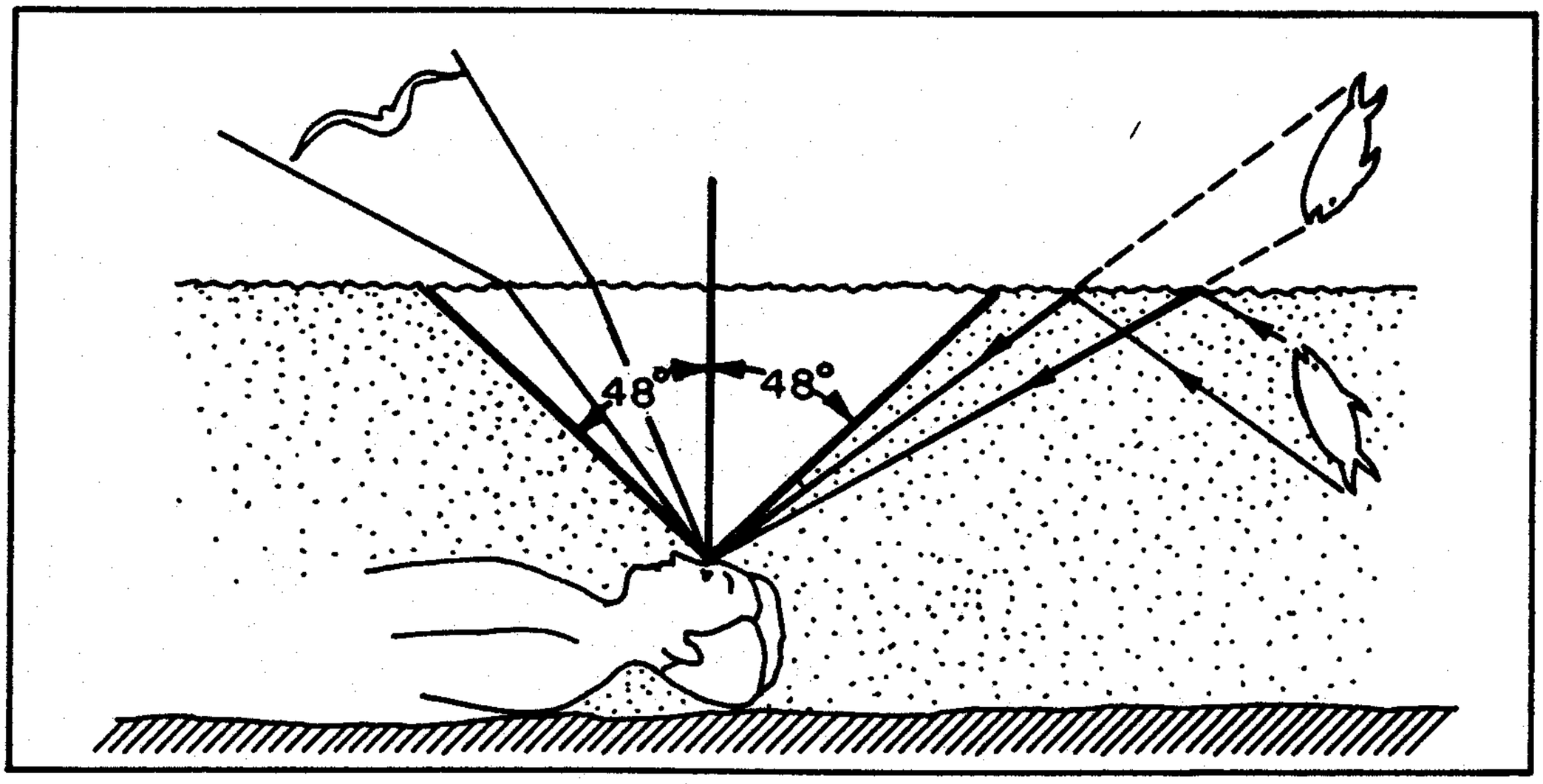

FIG. 1.18 The swimmer's optical manhole to the outside world.

following interesting account:

"As to the opacity of the ceiling, I thought it absolute until I threw my head back as far as I dared, [he was in an old fashioned iron helmet rig exploring Haiti Bay, in 1927] and saw, almost directly overhead, facets of clarity, appearing and vanishing, showing me an instant's patch of sky, a momentary glimpse of friend or boat--of that world to which it seemed at this moment inconceivable that I belonged. But anywhere except straight above me, the ceiling of the bay was watered gauze."

If the underwater observer now directs his attention downward, he may see in relatively shallow water a moving mosaic of bright and dark areas on the bottom, produced by the refracted sun's rays converging and diverging at various points on the bottom. When two bundles of rays are refracted so as to momentarily converge at a point A on the bottom (Fig. 1.19) the irradiance at A abruptly increases and is seen by the swimmer as a bright spot. On the other hand, rays could be diverted away from a point such as at B in Fig. 1.19, whereat it will be momentarily relatively dark. By knowing the statistics of the air-water surface slopes (as discussed above) it is possible to determine the statistics of the irradiance pattern on the bottom. The problem has recently been studied, e.g., by Redmond [260], and Schenck [272].

As one descends still farther, and if the water has a modicum of suspended and dissolved material which scatters light, the refracted rays of sunlight are then seen to form a pattern of moving beams and weaving, lighted, curtain surfaces very much like a watery aurora borealis or like the shafts of sunlight one sees directed earthward from rifts between clouds. These beams die away relatively quickly with depth in natural waters, at least as compared to the decay of the general diffuse light originating from the sky and clouds.

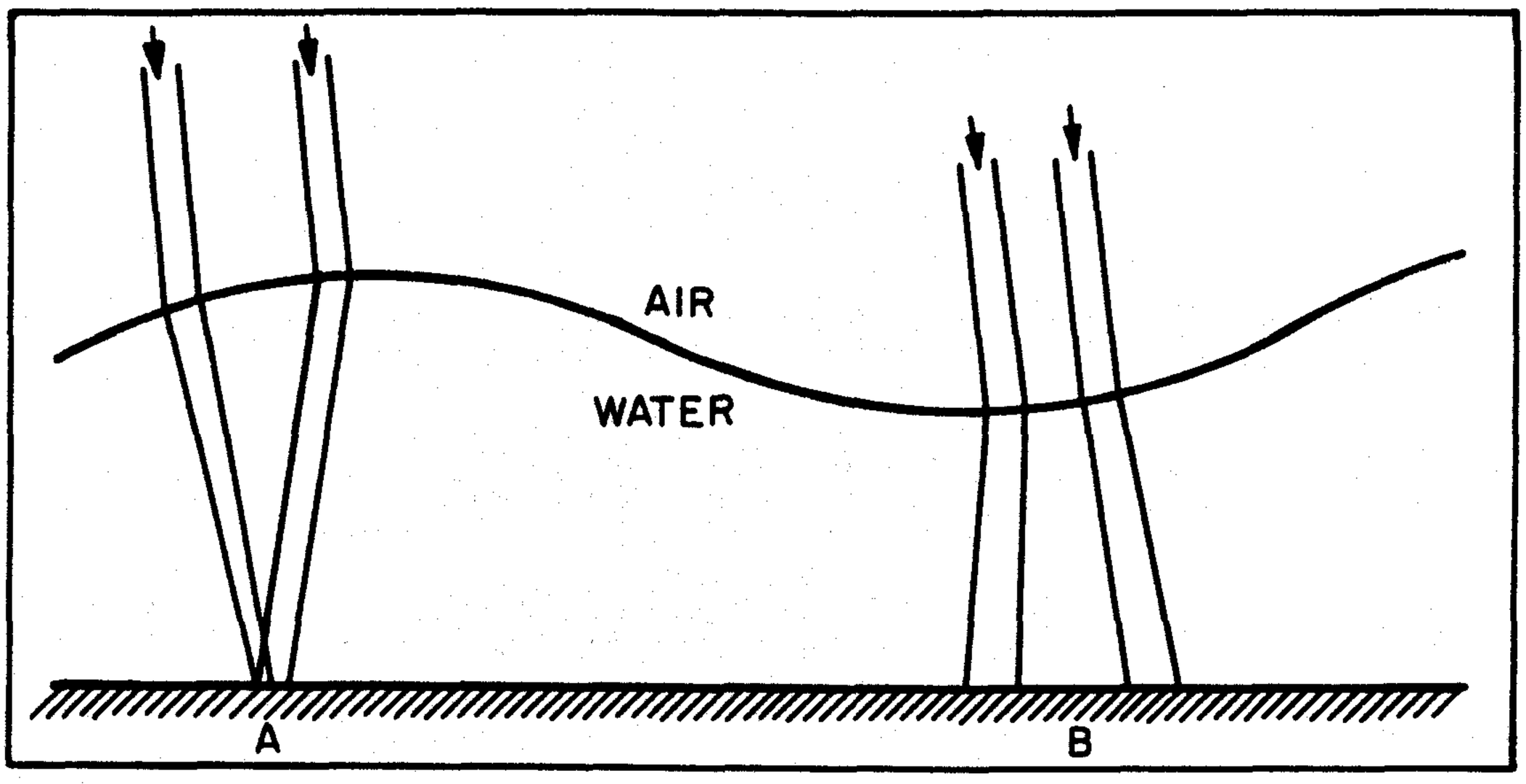

FIG. 1.19 Generating light patterns on shallow bottoms.

We shall look into this phenomenon in some detail later in this section.

One final subsurface refractive phenomenon we shall note here is that associated with the thermocline in natural hydrosols. The thermocline is the region of abrupt temperature change, (usually taking place in an extensive thin horizontal layer) found in most all natural waters, which separates a warmer layer from a cooler layer of water below it. It is detectable by means of a submersible thermometer known as a *bathythermograph*. Accompanying this temperature change is a corresponding density change of the water, and with this occurs a change in the refractive index of the water. Therefore we would expect some interesting refractive optical phenomena at the thermocline. Some observations of optical thermocline phenomena were made by Limbaugh and Rechnitzer [160] and are schematically summarized in Fig. 1.20, which is adapted from their paper. When the thermocline occurs in its more frequent guise, as a thin, horizontal, nearly motionless layer below the surface (as in the upper third of Fig. 1.20) one can actually see the thermocline from below as a smooth, nearly flat mirror-like plane boundary between the two water layers of differing temperature--and it generally manifests itself very much in the way the air-water surface does, even to the extent of having its own manhole into the warmer layer of water above. (Would one expect this manhole to subtend the same angular radius as the surface manhole?) Occasionally some rather unusual refractive phenomena may be observed when a moving tongue of cold water snakes its way through a warmer region on the bottom, (as in the lower left third of Fig. 1.20). The convex boundary of the tongue is visible all along its extent at grazing incidence, and its general appearance is reminiscent of the intertwining portions of two miscible liquids, such as clear alcohol and clear water. Finally, Limbaugh and Rechnitzer observed the optical thermocline effect in small isolated pools of relatively cold water resting

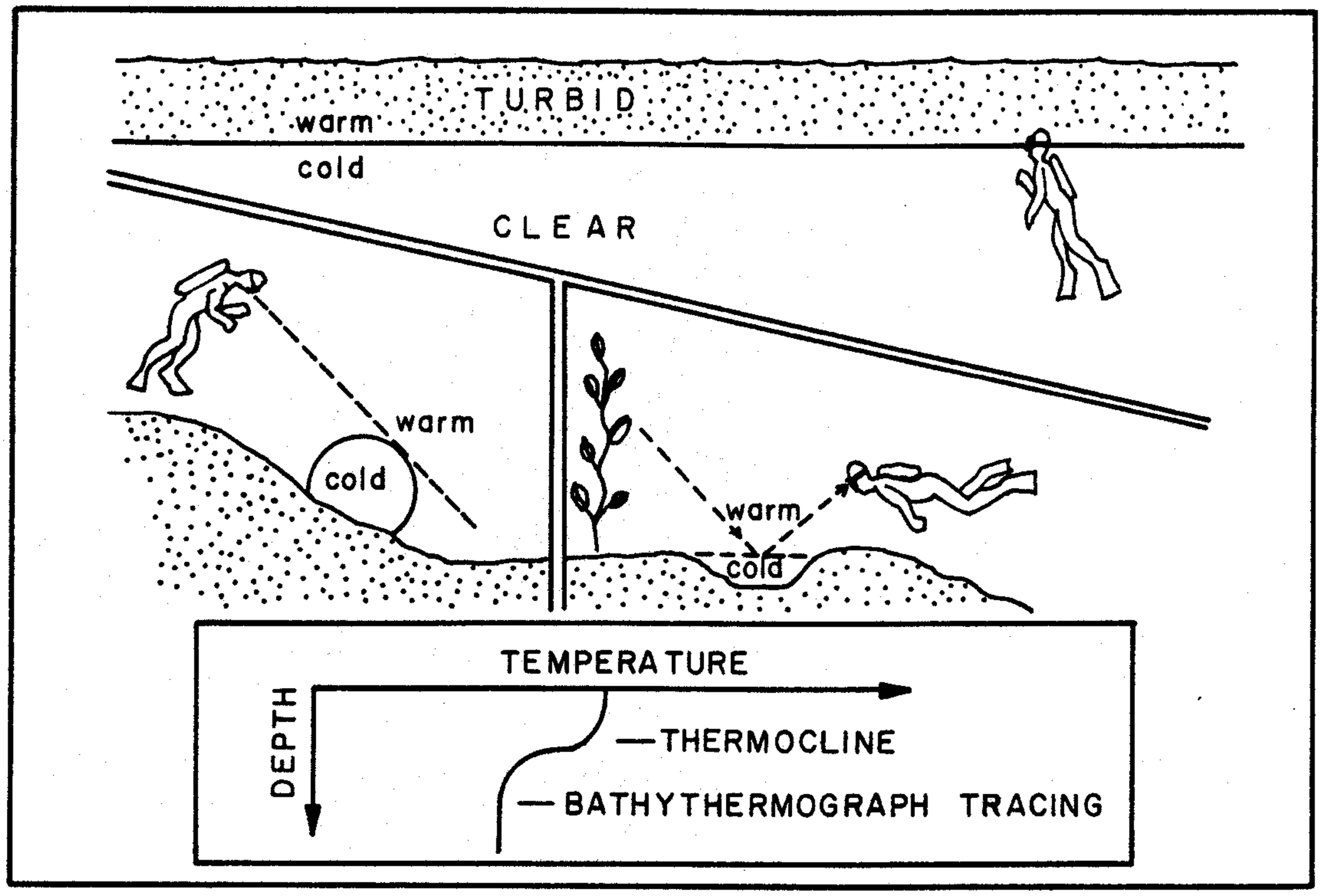

FIG. 1.20 Three interesting subsurface refractive phenomena. (From [160], by permission)

on the bottom in the midst of warmer water. These cool pools reflected light at their surfaces much in the way the still air-water surface reflects light for an observer above it.

The Decay of the General Light Field with Depth

Perhaps one of the most striking and outstanding features of the light field in deep natural waters is that it gets dark *fast* with increasing depth. For example infrared radiation (which comprises about half the irradiance at sea level on sunny noon days) is essentially absorbed in the first meter or so of most natural waters. There is a reasonably precise and simple law of darkening of the light field in this regard: the light field of any wavelength generally falls off or decays exponentially with depth. That is, if h(z) is the scalar irradiance at depth z in a homogeneous, deep lake or portion of the sea, then:

$$h(z) = h(0)\ e^{-Kz} \tag{7}$$

This type of law, namely the *exponential* type, is unquestionably the most ubiquitous of all types of natural laws in geophysics: it describes thermal and radioactive decay in solids and liquids, evaporation rates of falling rain droplets, growth rates of plant and animal species, fall off of atmospheric density with altitude, only to mention a few. In our

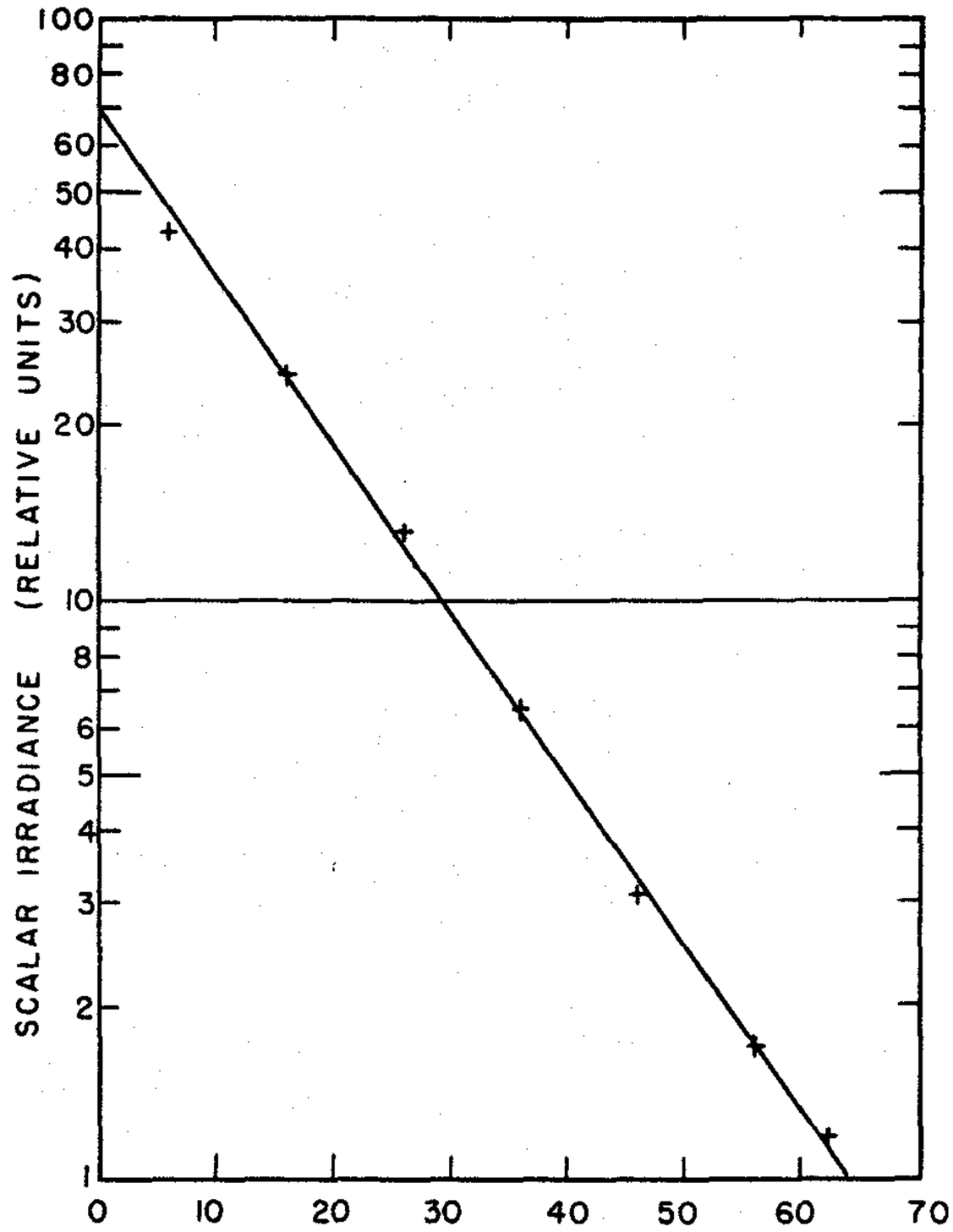

FIG. 1.21 Showing how scalar irradiance decreases exponentially with depth. Experiment by Duntley, Lake Winnipesaukee, N.H., September 1948. (Fig. 30, left diagram, from [78] by permission.)

present studies, it describes not only the decay of the natural light field with depth, but generally the decay of a beam of light with distance along its path. In the present case, the decay rate K depends on the wavelength λ of light considered ($h(z)$ depends on λ; however for brevity, as usual we omit "λ") and of course the clarity of the water considered. Indeed, as we shall see later, in Sec. 1.7, we may use the wavelength dependence of K to help classify the optical properties of natural hydrosols.

Figure 1.21 illustrates a sample experimental determination (taken from [78]) of the depth dependence of scalar irradiance in a deep clear lake (Lake Winnipesaukee, N.H.) over a depth range of 60 feet or 18.3 m. The crosses indicate the experimental points. The straight line is the best straight line for the data, and is plotted on semilog paper. The magnitude of the constant K is: $K = .066/ft. = .216/m$, for green light.

In view of the preceding observations there is no need at present of giving further graphs of $h(z)$ vs depth z in deep homogeneous media; for as the saying goes, 'if you have seen one, you have seen them all', the prototype being that displayed in Fig. 1.21. What is more worthwhile at present, is to raise such questions as: how is the exponential decay law affected if the medium is not deep, or if the bottom is clearly visible? What effects do inhomogeneities of the medium have on the exponential law? Does $h(z)$ decay at the

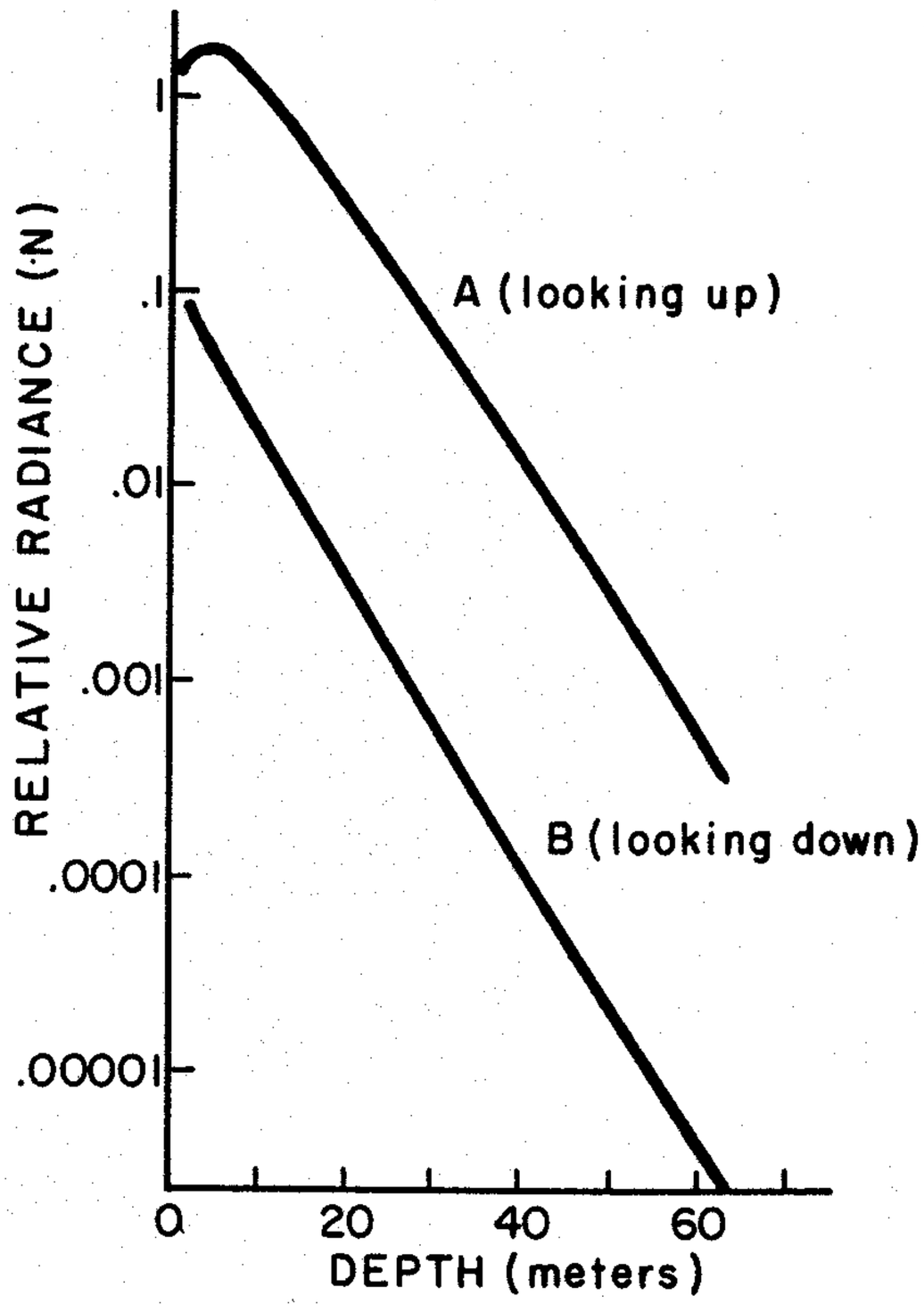

FIG. 1.22 Two experimental determinations of radiance by Tyler, Pend Oreille Lake, Idaho, April 1957. Note the general exponential decrease. Note, also, the slight buildup of radiance for the upward looking path near the surface. (From [298], by permission)

same rate at $H(z,\pm)$? (cf. (9) and (10) of 1.1). Does the exponential law hold right up to the surface, or is there a boundary effect? These and other questions are readily answered in detail by the theories developed in Chapter 8. Some simple answers are given in Sec. 1.4.

Behavior of Radiance Distributions with Depth

If we fix attention on the zenith radiance as we descend into the sea, then, aside from the effect on the radiance induced by a change of index of refraction (discussed above), there is observable a general build-up of radiance in the first meter or so below the surface. This build-up of light is depicted by Curve A of Fig. 1.22 (adapted from [298]) and is quite analogous to the increase in the light field one experiences as an airline passenger during the initial stages of the airliner's descent into a thick cloud layer lighted from above by the sun. We are observing in either case the storage of scattered radiant energy within the medium. In the case of the sea this increase in radiance is observable not only at the zenith, but in all upward looking directions, but is occasionally obscured by the refracted sunlight beams and other surface phenomena. The depth at which the maximum radiance occurs is predictable in theory and varies with the

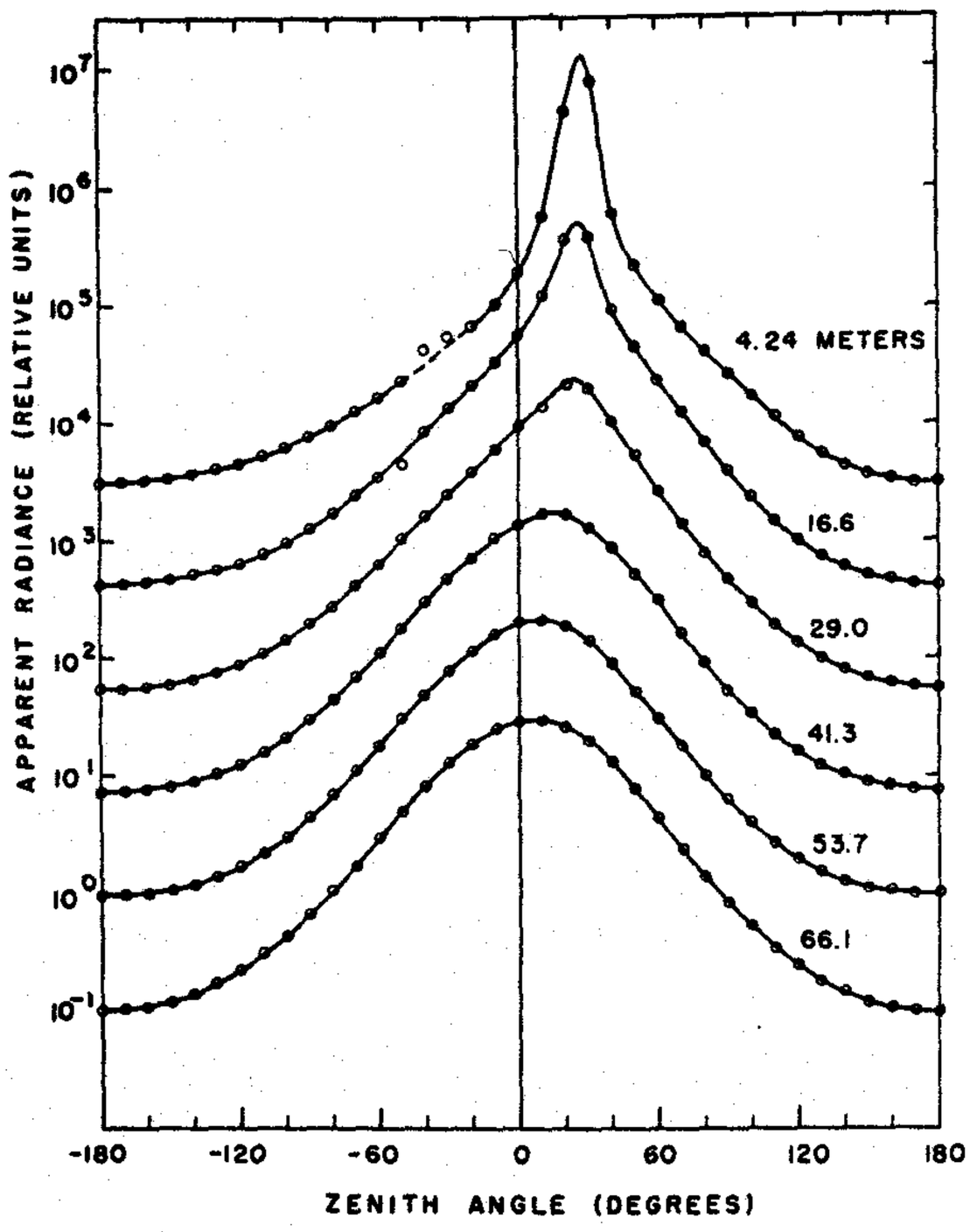

FIG. 1.23 Radiance distributions, in the vertical plane containing the sun, on a clear sunny day, at the indicated depth, in Lake Pend Oreille, Idaho, as measured by Tyler, April 1957. Observe how the shapes of the curves become similar as depth increases. (Fig. 26, from [78], by permission)

direction of sight and the clarity of the medium (cf. (12) of Sec. 4.4).

After the maximum radiance occurs in a given direction, the radiance in that direction begins to fall off rapidly with depth and soon assumes the exponential behavior that h(z) universally exhibits. This trend to exponentiality is seen quite clearly in the nadir curve B of Fig. 1.22, or more generally in Fig. 1.23, which is adapted from [78]. Fig. 1.23 is designed to show how the *shapes* of the radiance distributions vary with depth in the hydrosol. The particular graphs in Fig. 1.23 are adapted from [78] and represent the light field measured in Lake Pend Oreille, Idaho by Tyler [298]. The radiance is associated with a wavelength of 480 ± 64 mμ, in water with a K of about .170/m and (for future reference) an α of .370/m. Two important and universal properties of underwater radiance distributions are discernable in this set of curves: (i) the decrease in peakedness of the curves with depth, accompanied by a trend toward a limiting shape as depth increases, and (ii) the shift of the radiance maxima toward the zenith with increasing depth. Near the surface the peaks are pointed toward the refracted image of the sun; but this orientation is lost as depth increases. This trend toward a stable vertically-oriented smooth distribution is shown in more detail in Fig. 1.24, wherein the zenith angles of the maxima in Fig. 1.23 are plotted as a

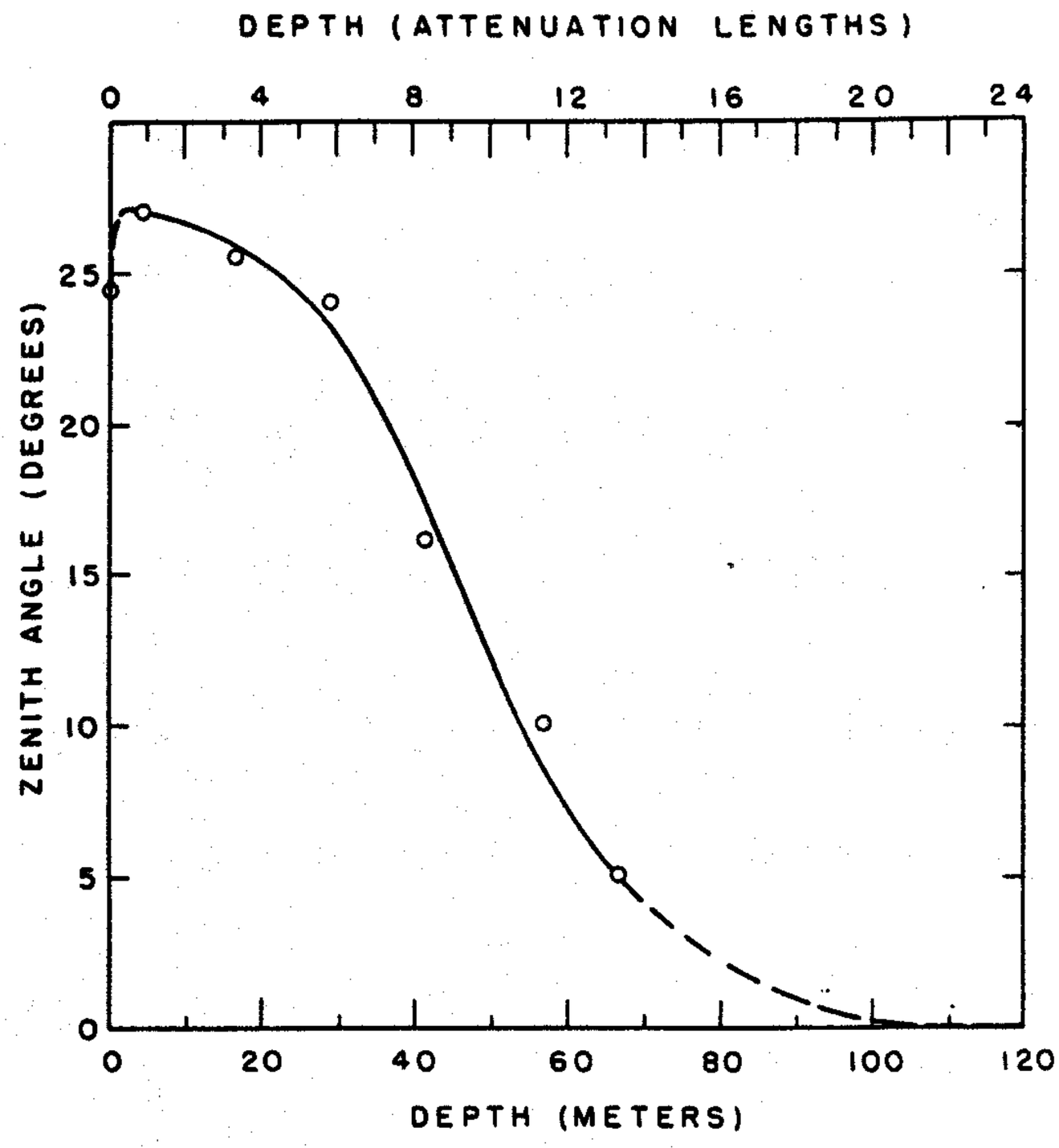

FIG. 1.24 Plot of zenith angle of the maxima of the curves of Fig. 1.23. The maxima shift toward the zenith with increasing depth. This figure and Fig. 1.23 present graphic evidence of the validity of the asymptotic radiance hypothesis. (Fig. 28 from [78], by permission)

function of depth. The problem of the description of the depth dependence of the radiance distribution in natural hydrosols is one of the principal tasks of hydrologic optics and to which much of this work is devoted.

The Asymptotic Radiance Hypothesis

The fact that the shapes of the radiance distributions in deep hydrosols approach limiting forms with increasing depth is observable in Both Figs. 1.23 and 1.24. In the former figure all the radiance curves eventually steady in shape with increasing depth. This means that eventually all radiances are decreasing at the same exponential rate with depth. Hence the evidence points to the fact that radiance distributions eventually assume certain stable shapes and these distributions subsequently shrink down exponentially in size with increasing depth, all the while preserving those shapes. The general statement of the existence of such limiting shapes in all homogeneous natural hydrosols is the *asymptotic radiance hypothesis* which was first clearly enunciated by Whitney [315] on the basis of experimental findings, and subsequently proved mathematically in [225]. The validity of the asymptotic radiance hypothesis has important consequences for the development of simple theoretical models of the light field

in the sea and in deep lakes, rivers and harbors. For example the scattering and absorption functions in the general theory depend in part on the shape of the radiance distributions. If these distributions do not vary too much with depth, vast simplifications of the general theory are possible. These matters will be pursued at some length in Chapters 6, 8 and 10.

Underwater Irradiance Distributions

The studies of visibility and biological problems--as far as they are concerned with the radiometric environment--are facilitated by knowledge of the irradiance distributions $H(z,-)$ at each depth z in the medium of interest. Figure 1.25, plotted from the tables in [304], illustrates such a distribution as a function of orientation of the collecting surface's outward normal direction (θ,ϕ) and also of depth, for a sun zenith angle of 33.4°. This graph keys in with that of Fig. 1.23, being the irradiance distribution computed from the radiance distributions in Fig. 1.23, using (1) of 1.1. The role of (θ,ϕ) is depicted in Fig. 1.26.

It is of both practical and theoretical interest to know that an irradiance distribution $H(z,\cdot)$ at a depth z contains just as much information as the radiance distribution $N(z,\cdot)$ at that depth. This will be shown in Ex. 15 of Sec. 2.11, wherein knowledge of N will be used to deduce knowledge of H, and conversely. The bridge between $N(z,\cdot)$ and $H(z,\cdot)$ is easily traversed in the direction $N \to H$ but is somewhat more difficult to traverse numerically in the direction $H \to N$, and until an efficacious numerical scheme to bridge the latter gap is devised, the radiance distribution will continue to be measured and be the favored means of cataloging natural light fields.

Some practical features of irradiance distributions are as follows. Every irradiance distribution satisfies the exact cosine law:

$$\overline{H}(z,\xi) = \overline{H}(z,\mathbf{m}) \cos\theta$$

where $\overline{H}(z,\xi)$ is the net irradiance in the direction ξ, $\mathbf{m}$ is the direction of greatest net irradiance (cf. (14) of Sec. 2.8), and θ is the angle between ξ and $\mathbf{m}$. This law shows that we need only plot or tabulate irradiance distributions $H(z,\cdot)$ for directions ξ not greater than 90° away from some arbitrary fiducial direction, say the vertical direction $\mathbf{k}$. To see this, suppose that we have $H(z,\mathbf{k})$ and $H(z,-\mathbf{k})$ and that we know $\mathbf{m}$. Then by the exact cosine law:

$$\overline{H}(z,\mathbf{k}) = H(z,\mathbf{k}) - H(z,-\mathbf{k}) = \overline{H}(z,\mathbf{m}) \cos\theta_{\mathbf{m}} \qquad (8)$$

where $\theta_{\mathbf{m}}$ is the angle between $\mathbf{k}$ and $\mathbf{m}$. From this we can compute $\overline{H}(z,\mathbf{m})$. Now suppose we know $H(z,-\xi)$ and that we want to know $H(z,\xi)$, where ξ is less than 90° from $\mathbf{k}$. Then the

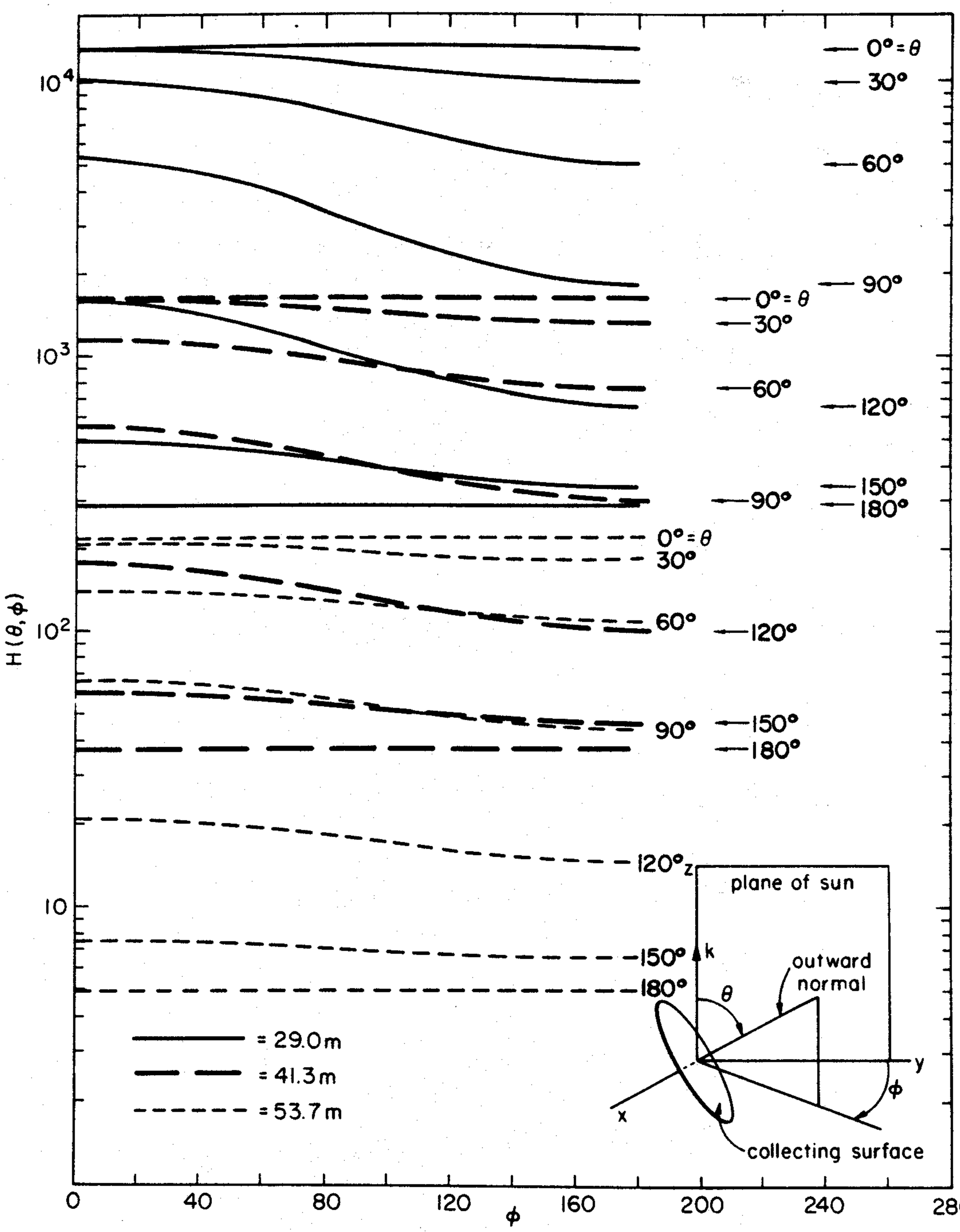

IRRADIANCE DISTRIBUTION (H) CLEAR, SUNNY SKY

FIG. 1.25 Irradiance distribution on a clear sunny day at the indicated depths, in Lake Pend Oreille, Idaho, 28 April 1957, as computed by Schaules and Tyler from Tyler's data.

FIG. 1.26 The collecting surface receiving the irradiance recorded in Fig. 1.25.

cosine law yields:

$$H(z,\xi) = H(z,-\xi) + \bar{H}(z,\mathbf{m}) \cos\theta \tag{9}$$

Therefore knowledge of $\mathbf{m}$ and $\bar{H}(z,\mathbf{m})$ together with $H(z,\cdot)$ over one hemisphere of directions, will yield $H(z,\cdot)$ over the remaining hemisphere.

Another practical aspect of the irradiance distribution is that is can be used to compute one of the basic optical properties--namely the volume absorption function, a --of natural optical media, by using the *divergence law*:

$$\frac{d\bar{H}(z,\mathbf{k})}{dz} = a(z)\, h(z) \tag{10}$$

for the vector irradiance (cf. (1) of 13.8, and Sec. 1.4 below). Thus knowledge of $H(z,\cdot)$ leads to $\bar{H}(z,\mathbf{k})$ and to the latter's derivative by straightforward computations. This, together with auxiliary determinations of h, yields estimates of a.

Subsurface Contrast Reduction by Scattering and Absorbing Effects

Underwater scenes in seas, lakes and harbors are characteristically dim and blurry. The sharp outlines and stark contrasts above the surface are relatively absent from underwater scenes. Even in the clearest swimming pools, distant objects no longer have sharp edges, and contrasts are slightly but yet noticeably decreased. If one looks a bit closer at these contrast-reduction phenomena, one outstanding and fundamental fact soon becomes manifest: on the one hand, as the observer recedes from a relatively bright object, its luminance rapidly falls off and soon melts into the background luminance; on the other hand, if the object is relatively dark, its luminance rapidly increases with viewing distance and eventually also melts into the background luminance. Is there some order and regularity in these changes of apparent contrast with viewing distance? In other words is there some general law followed by these changes in apparent contrast of distantly viewed objects in underwater scenes? The answer is 'yes', provided a judicious scientific choice is made in the selection of the notion of *contrast*.

If ${}_tN_r$ is the apparent (surface) radiance of an object (the *target*) viewed at a distance r underwater, and ${}_bN_r$ is the apparent (surface) radiance of its background, then we write

$$\text{"}C_r\text{"} \quad \text{for} \quad ({}_tN_r - {}_bN_r)/{}_bN_r \tag{11}$$

and call C_r the *apparent contrast* of the target with respect to its background. The geometry of this situation is pictured in Fig. 1.27. If r=0, we call C_o the *inherent contrast* of the

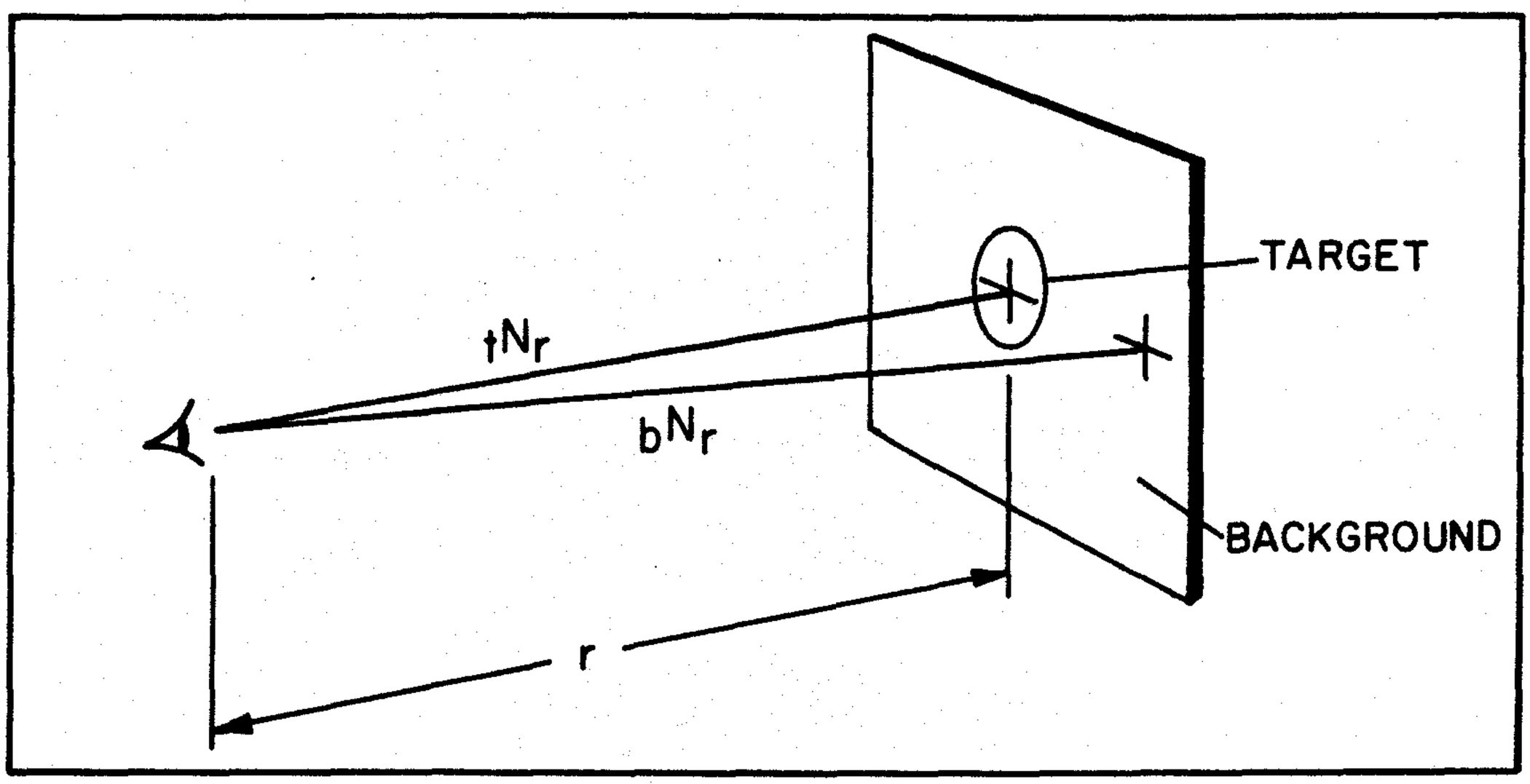

FIG. 1.27 The apparent contrast of a target against its background.

target with respect to its background.

Figure 1.28 shows an experimental arrangement, devised by Duntley [78], to study contrast reduction phenomena in Lake Winnipesaukee, N.H.. A telephotometer (i.e., a radiant flux meter attached to a telescope) was mounted on a small, hooded glass-bottomed boat which looked at a flat white target at depth r. At the time of the experiment (sometime in September 1948) the water was calm, the sky was clear, with a low sun. For later reference we will note that the lake at that time had a K of 0.216/m and an α of 0.594/m, for green light. The observation of interest at the moment is recorded in Fig. 1.29, in its original form, which shows the sought-for law governing C_r vs distance r in feet. This clearly shows an exponential decrease of C_r with r, in this case depth r below the bottom of the boat. In fact it was found, on converting to meter lengths, that:

$$C_r = C_o\, e^{-.810\ r} \quad .$$

This finding of the exponential law is in itself a remarkable one; however, the really exciting fact lay in the nature of the number .810/m(=.247/ft), the exponential decay rate of the apparent contrast. It was found that:

$$.810 = .594 + .216 = \alpha + K \quad \text{(per meter)}$$

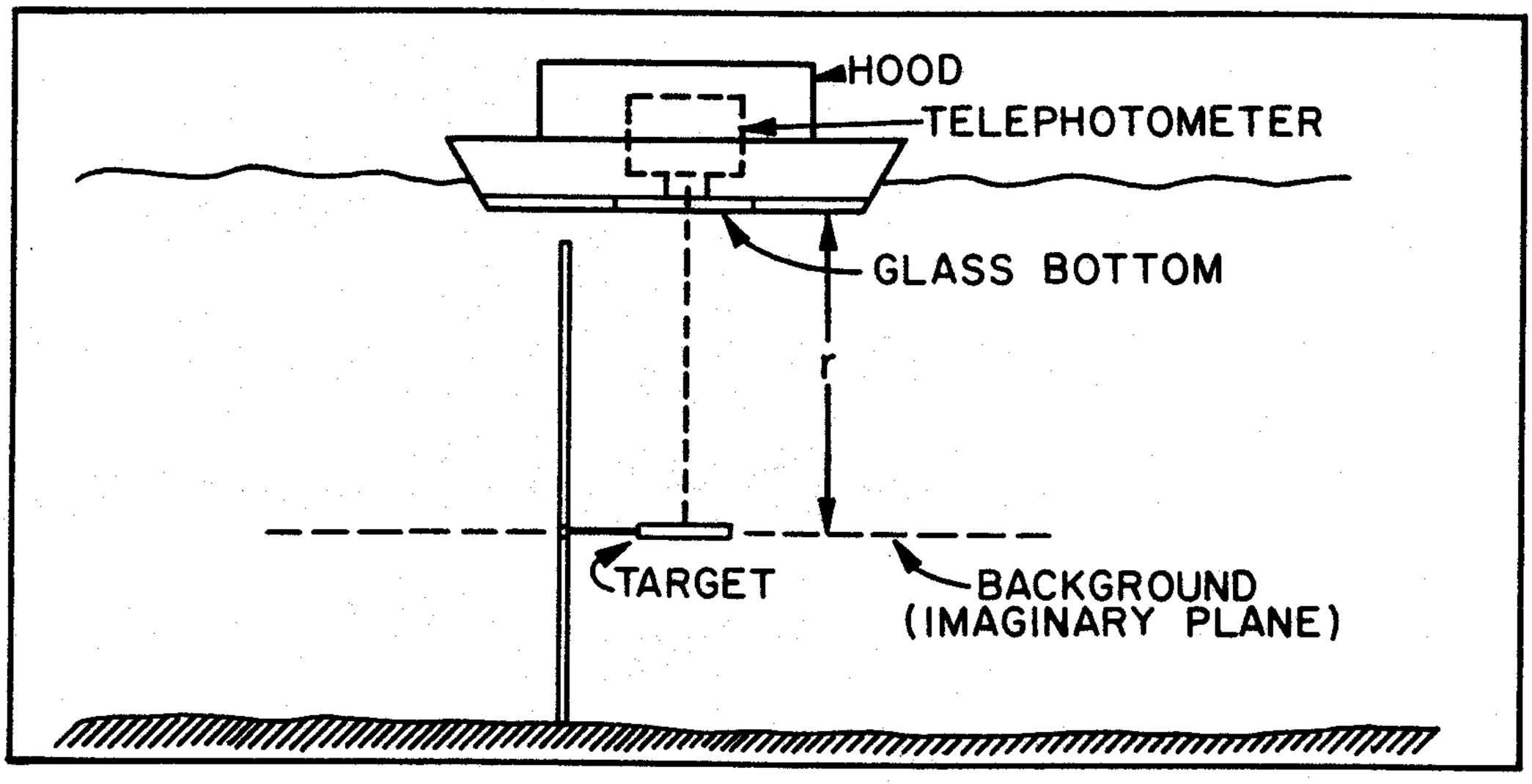

FIG. 1.28 Physical set-up for Figs. 1.29, 1.30.

To see the significance of this, recall our earlier observations on the general mode of decay of the natural light field in the water. The depth rate of decay is given by K. The α on the other hand, gives the depth rate of decay of a beam of light in the water. Therefore there are two mechanisms involved here in giving rise to contrast reduction. These are summarized by K and α, and are generally distinct. These will share our attention later. But for the moment we quietly revel in the presence of discerned order in at least one feature of the underwater radiometric environment. It was perhaps this experimental finding and the ones immediately following it, shown in Fig. 1.30, that contributed more than any others, to inspire Duntley and one of his students (the present author) to turn to the problem of explaining these interesting (and then, mysterious) manifestations of order in the submarine light field, and relating them to the general radiative transfer phenomena in scattering-absorbing media.

What is shown in Fig. 1.30 (which holds for the same setting as above) is an extension of the findings in Fig. 1.29, and once again in the original form given by Duntley. The new figure shows several things. First, it shows that the apparent contrast of an object is exponentially attenuated with target distance at the same space rate for both light and dark targets. Second, this space rate is independent of azimuth of the line of sight (here, the direction of motion of the photons) which in this experiment was inclined at an angle θ of 30° away from vertically upward, or an amount $\theta = 150°$ from vertically downward. (See Fig. 1.31) In particular the azimuths, measured from the vertical plane of the sun, are

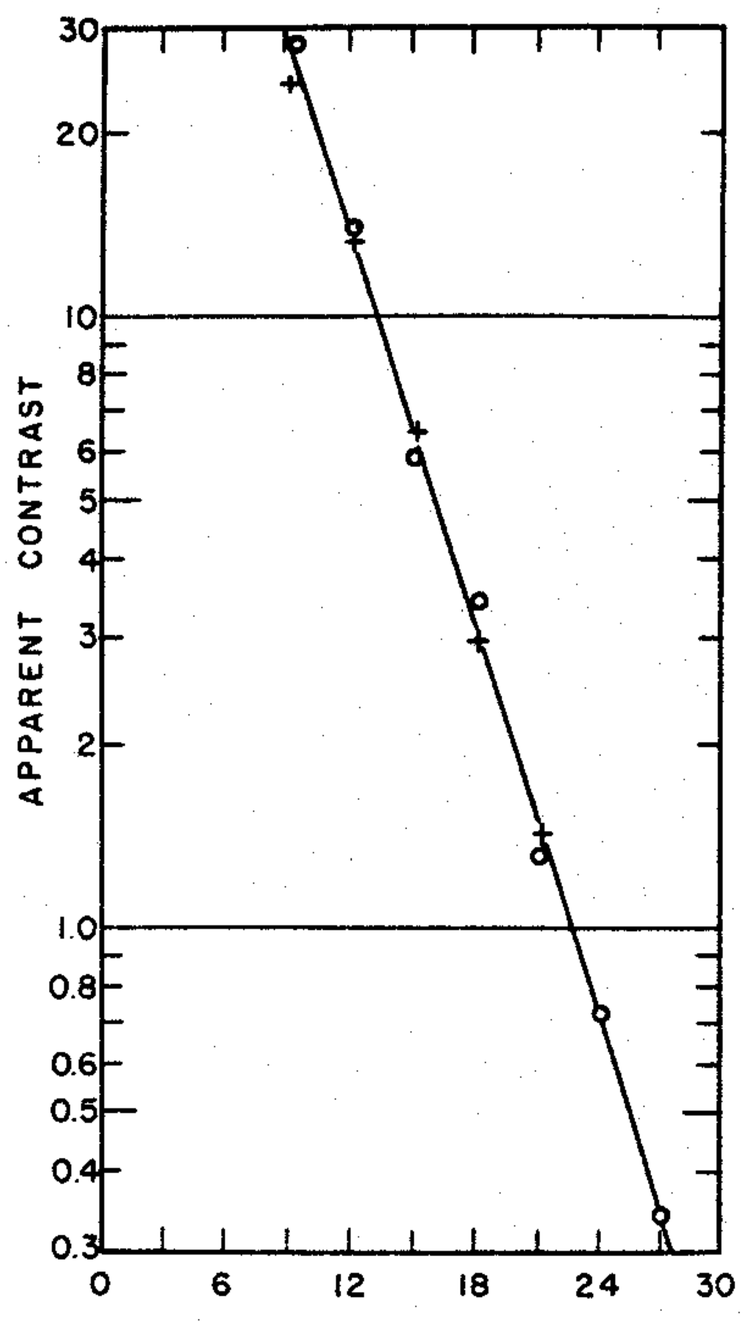

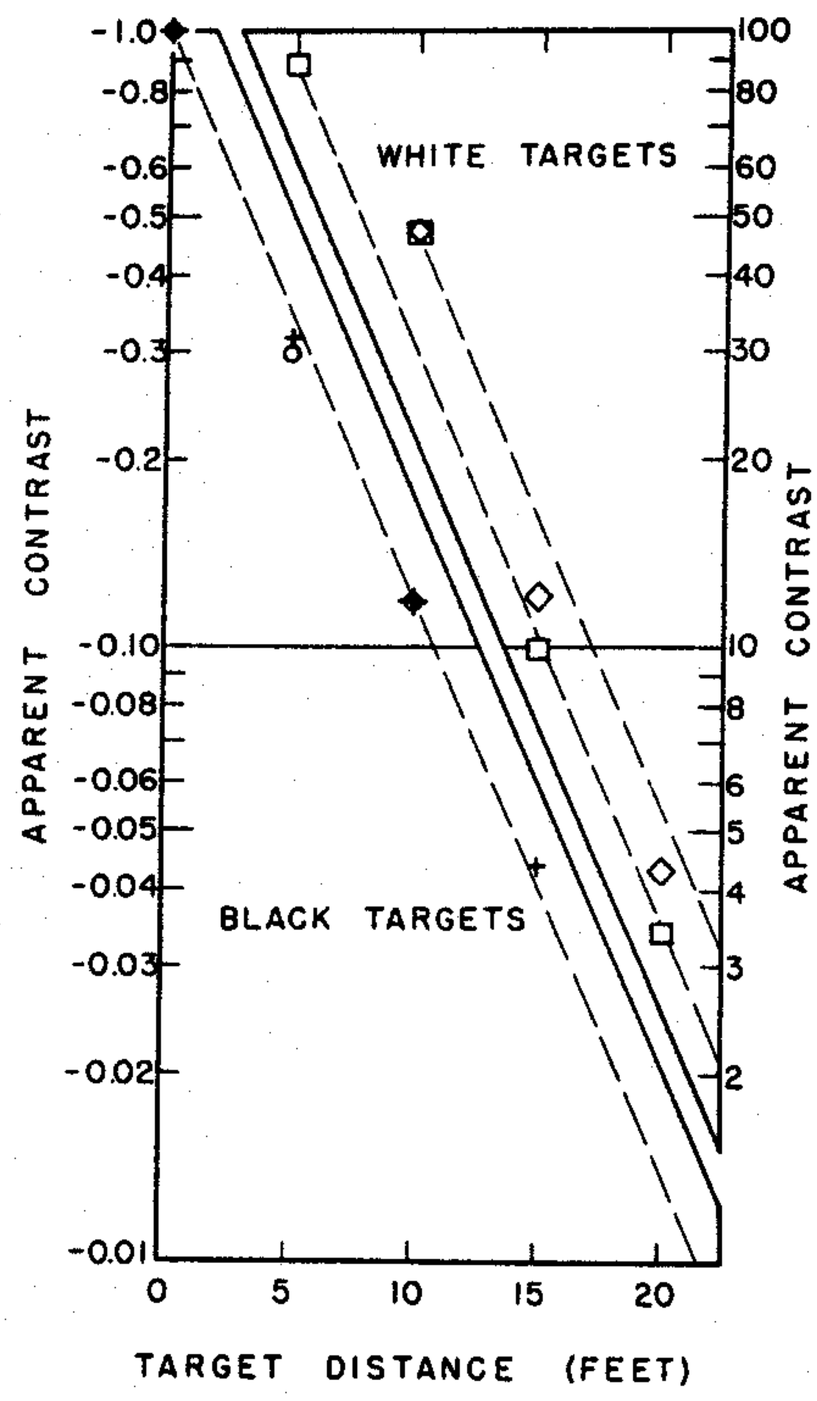

FIG. 1.29 Duntley's classic experiment showing the exponential law of decrease of apparent contrast along a vertical path in a natural hydrosol (Lake Winnipesaukee, N.H., Autumn, 1948. See also Figs. 1.28, 1.30)(Fig. 30, middle diagram, from [78], by permission)

FIG. 1.30 Further experimental evidence for the exponential apparent contrast law. (See Figs. 1.29, 1.31)(Fig. 30, right diagram, from [78], by permission)

$\phi = 0°$ (circled points), $\phi = 45°$ (crosses), $\phi = 95°$ (diamonds) and $\phi = 135°$ (squares). The dashed straight lines are drawn parallel to help judge the slope and linearity of the data and have a natural logarithmic slope of about .781/m. Once again this exponential decay rate is a source of surprise when it is observed that

$$.781 = .594 + .216 \cos 30° \quad \text{(per meter)}$$

This would lead one to conjecture that paths of sight inclined generally at θ from the vertical in homogeneous stratified media, as shown in Fig. 1.31, would have an apparent contrast C_r associated with them of the general form

$$C_r = C_o\, e^{-(\alpha + K \cos \theta) r} \tag{12}$$

The conjecture was confirmed and a simple theoretical model underlying this contrast reduction law was soon evolved. The model will be discussed further in Sec. 1.4, in Chapter 4, and Chapter 9.

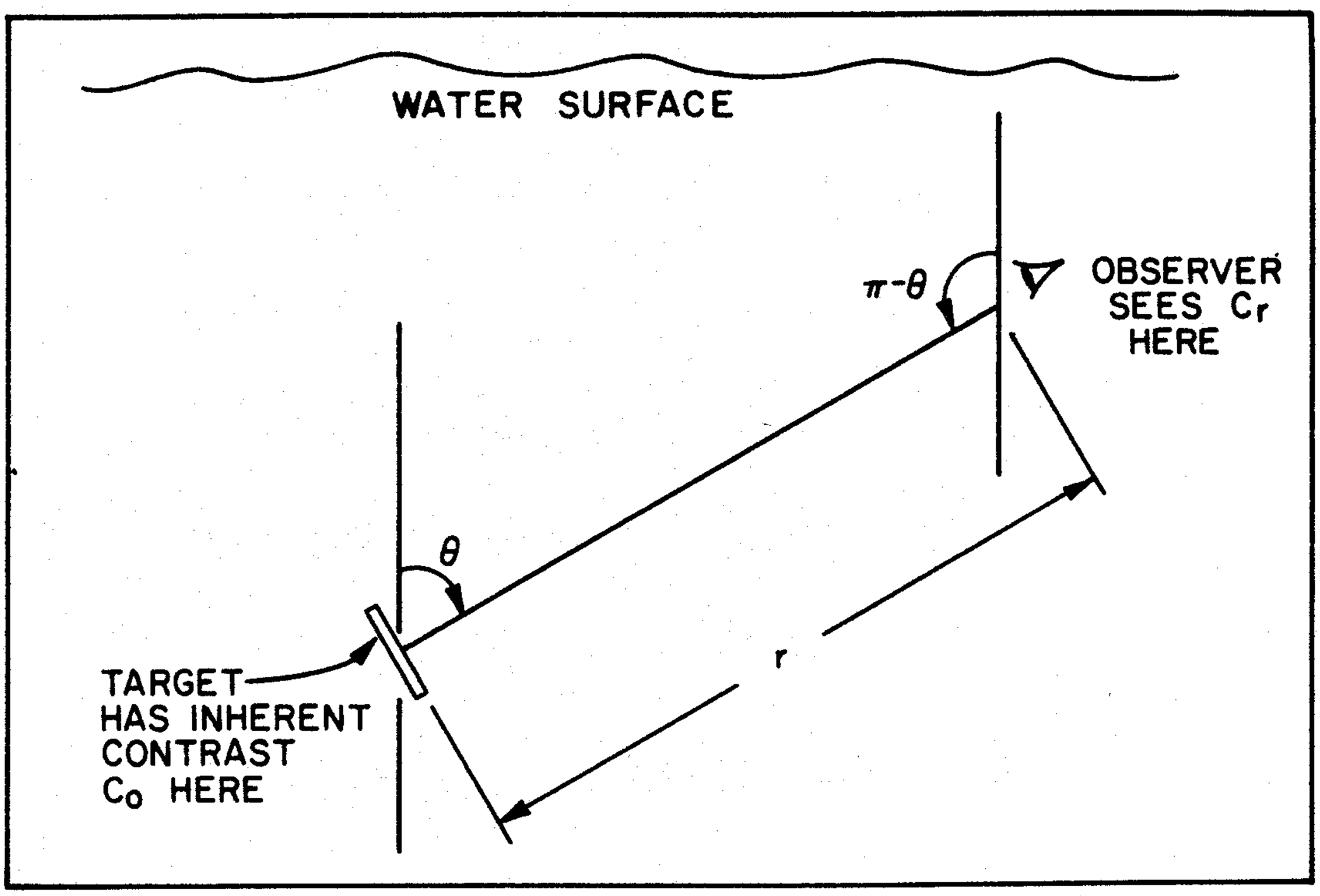

FIG. 1.31 The geometrical details for Fig. 1.30, in which $\theta = 30°$.

Subsurface Contrast Reduction by Refractive Effects

When one looks across an extensive flat stretch of the earth's surface such as a meadow or stretch of ocean on a sunny or very windy day, distant objects seem to be blurred not only by the usual atmospheric haze, but also by a rapidly varying shimmering or "heat wave" effect. This phenomenon is produced by inhomogeneities of the refractive index of the air along the line of sight and is associated with cells of air of different density. These in turn are related to uneven temperature distributions in the air mass or simply to the local mechanical compression of the air in gusts of wind on windy days. The same mechanism makes the stars twinkle at night.

It may come as a mild shock to some observers to occasionally see this same twinkling, heat-wave like effect in the otherwise cool depths of an incompressible fluid like a sea or a lake. Nevertheless, the effect exists, and on closer examination, sanity prevails: the underlying mechanism is seen to be refractive, but produced by myriads of tiny transparent plankton, whose indices of refraction differ very slightly from that of water. In some south sea waters, it is said that the concentration of such plankton is so great, the spacing between a swimmer's toes cannot be distinguished by him, though the foot is visible with high contrast against its background. A somewhat less dramatic but similar phenomenon was observed and recorded by Duntley at the Diamond Island Field Station in Lake Winnipesaukee, N.H.. Figure 1.32, from [78], shows a photograph of the light distribution on a camera

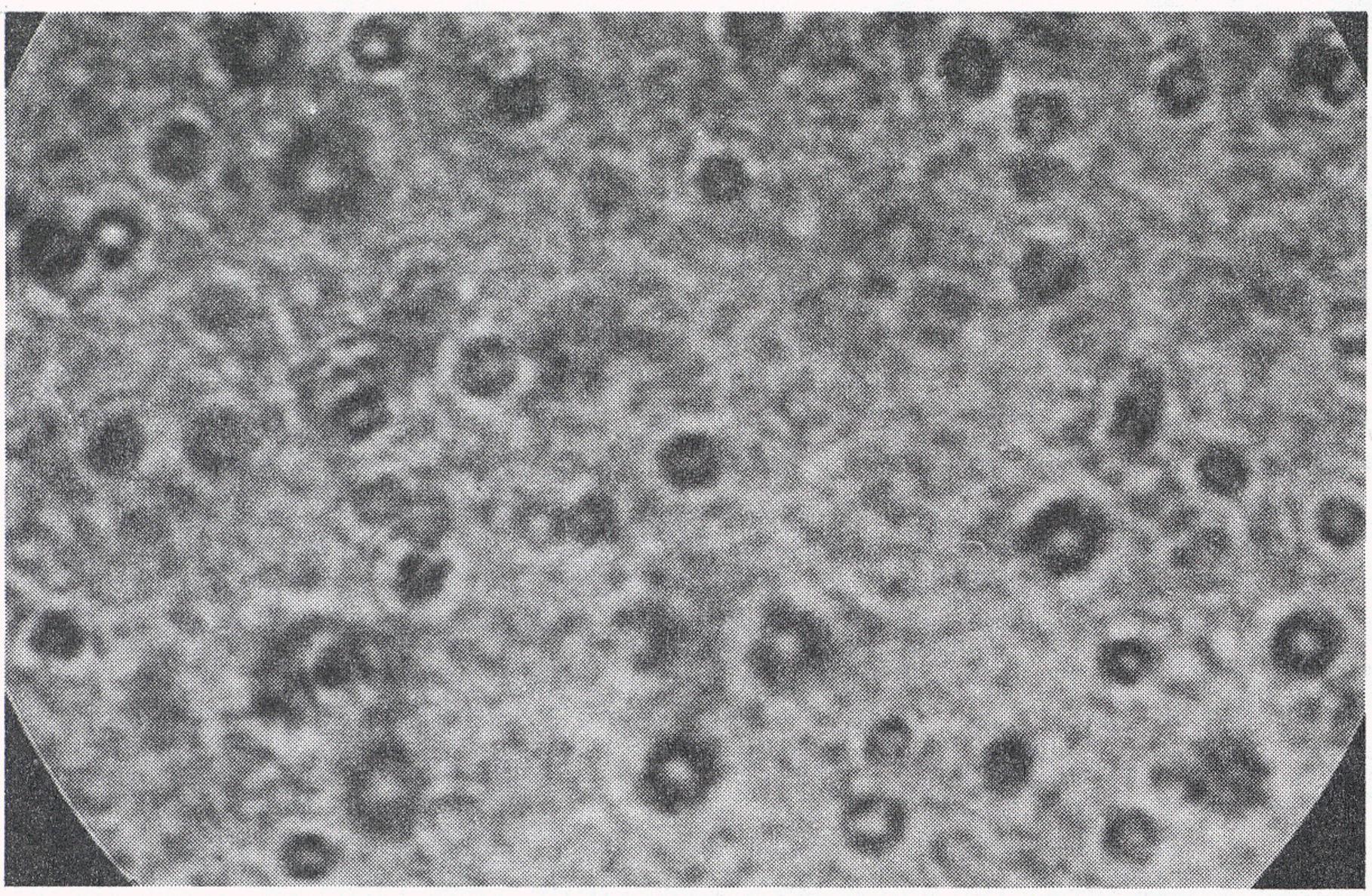

FIG. 1.32 Swarming plankton photographed in the light of a strong collimated beam, as observed by Duntley in Lake Winnipesaukee, N.H., 22 August 1961. Plankton swarms such as these may contribute to contrast reduction along underwater paths of sight. (Fig. 22 from [78], by permission)

FIG. 1.33 Arrangement for plankton photograph, Fig. 1.32. (Fig. 21 from [78], by permission)

film produced by a collimated light beam after having travelled through a horizontal 3 m water path shown in Fig. 1.33. The time of year was late August (1961) and the exposure time was 1/50 sec. on an Eastman Plus-X film with a normal D-76 development. The beam had a diameter of about 5 cm and a

spread of about 0.01°. The α of the water was .585/m, in green light. The water path between the lamp and camera was swarming with plankton, and the bright collimated beam has limned some of these on the photographic film. To judge the size of these tiny organic refractive cells, the diameter of the black circular border (caused by the camera opening) was measured to be 3.3 cm on the negative.

A theory for the loss of contrast of objects seen through atmospheric boil was evolved some time ago by the author and some of his colleagues [81]. This theory appears to be applicable also to the contrast reduction phenomenon described above. The effect, however, is generally mild when it does occur, and may for virtually all practical purposes be ignored in the problem of predicting underwater visibility. However, in passing we may note that in a natural hydrosol which has such transparent plankton distributed uniformly and densely along a path of sight of length r the theory predicts that the magnitude of the blur (the standard deviation of the angular displacement of a typically straggling light ray from observer to object plane) increases like $r^{1/2}$ and the apparent contrast of fine details in an object against the general background decreases like $1/r^3$. Thus the contrast reduction law produced by refractive inhomogeneities in a medium is, on the one hand, quite different from that produced by scattering-absorbing mechanisms in that medium, and summarized in (12). On the other hand, as a perusal of [81] would show, the theory of the present effect is quite close to that used to derive (5).

The Polarization of Underwater Light Fields

Up to now we have been describing those optical effects in natural hydrosols that have very little directly to do with the fact that photons, in their pristine state, are viewable as particles with observable spins--i.e., with an observable property we usually call *polarization*. If we now invoke the quantum theoretical wand of complementarity and imagine the photon to be not a small, hard, colored ball but, rather a relatively compact packet of electromagnetic waves whose **E** and **H** vectors vibrate in fixed mutually orthogonal planes as the packet moves along (see Fig. 1.34), then we add a new dimension to the description of radiometric phenomena. No longer is it sufficient to merely describe the unpolarized radiance of the light field, but rather we must go on to describe radiance carried by those photons at x in the direction ξ whose **E** vector is oriented by the general angle ψ with respect to some reference frame.

Suppose we place a polarizer into the radiance tube, as shown in Fig. 1.35. (Compare with (b) of Fig. 1.5.) This may be made from some commercially available polaroid material. Then if we fix x and ξ as usual, and rotate the polarizing element, we can detect the presence of polarized radiance by the varying output of the radiant flux meter's dial. Suppose we turn the polarizer one full turn. Let $N_{max}(x,\xi)$ and $N_{min}(x,\xi)$ be the maximum and minimum radiances so obtained.

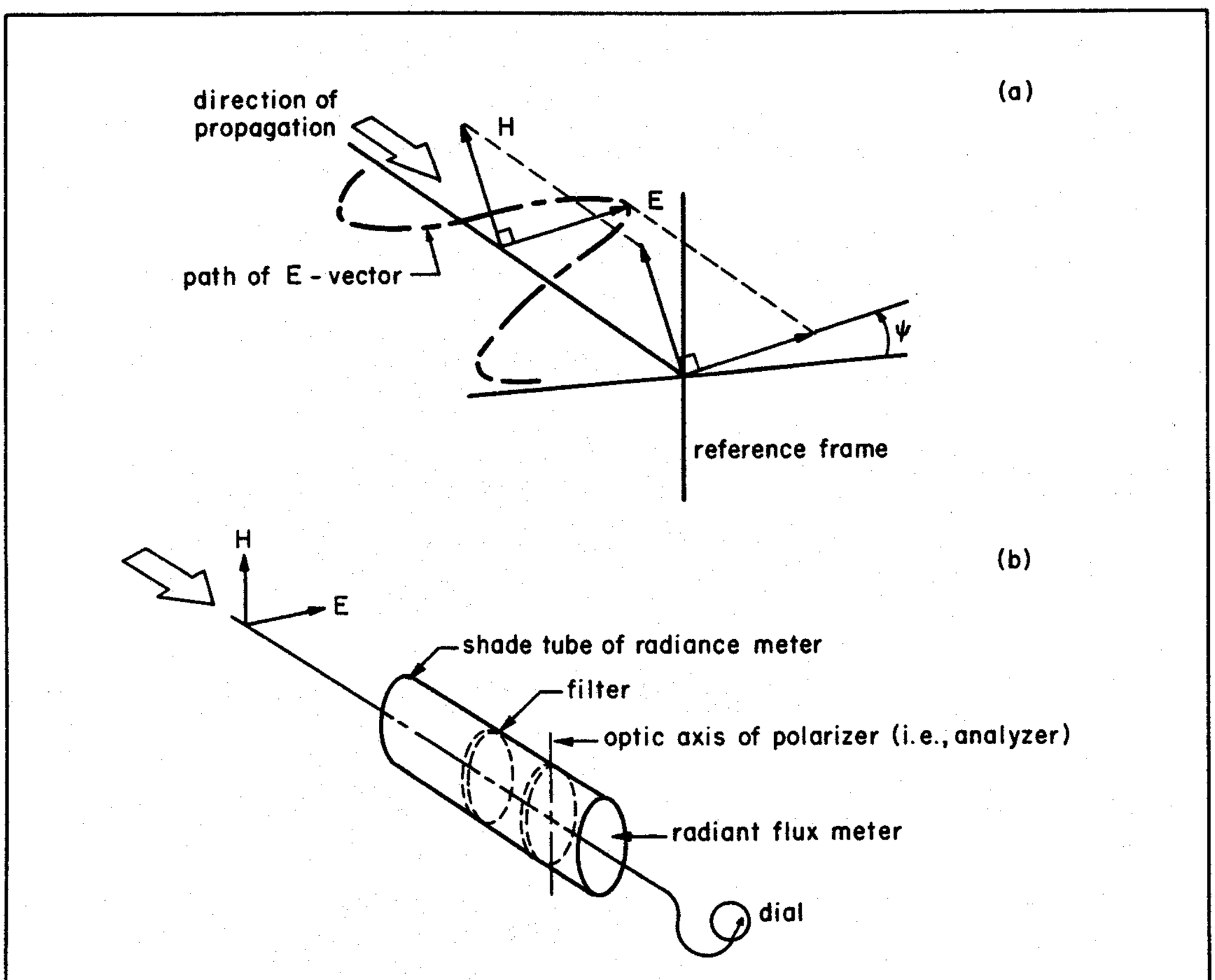

FIG. 1.34 A linearly polarized E-vector.
FIG. 1.35 The placement of a polarizer in a radiance tube preparatory to measuring the polarization of a light field.

Then we write

$$\text{"p}(x,\xi)\text{"} \quad \text{or "p"} \quad \text{for} \quad \frac{N_{max}(x,\xi) - N_{min}(x,\xi)}{N_{max}(x,\xi) + N_{min}(x,\xi)}$$

$p(x,\xi)$ is called the *polarization* of the light field at x in the direction ξ, and is a useful measure of how much polarization is present in the light field at x.

Now if we train such a polarized radiance meter at a clear sky, we find that the sky radiance is most noticeably polarized in all directions which lie in a plane normal to the direction of the sun's rays. If we go below the air-water surface we find that the light field is still polarized but to a lesser extent. The shafts of sun and skylight beaming down into and around the manhole (described above) are *scattered* into the line of sight by the water in a manner completely analogous to the sunlight streaming into and scattering within the upper atmosphere. Furthermore, the underwater light field may also be reflected into the line of sight by the underpart

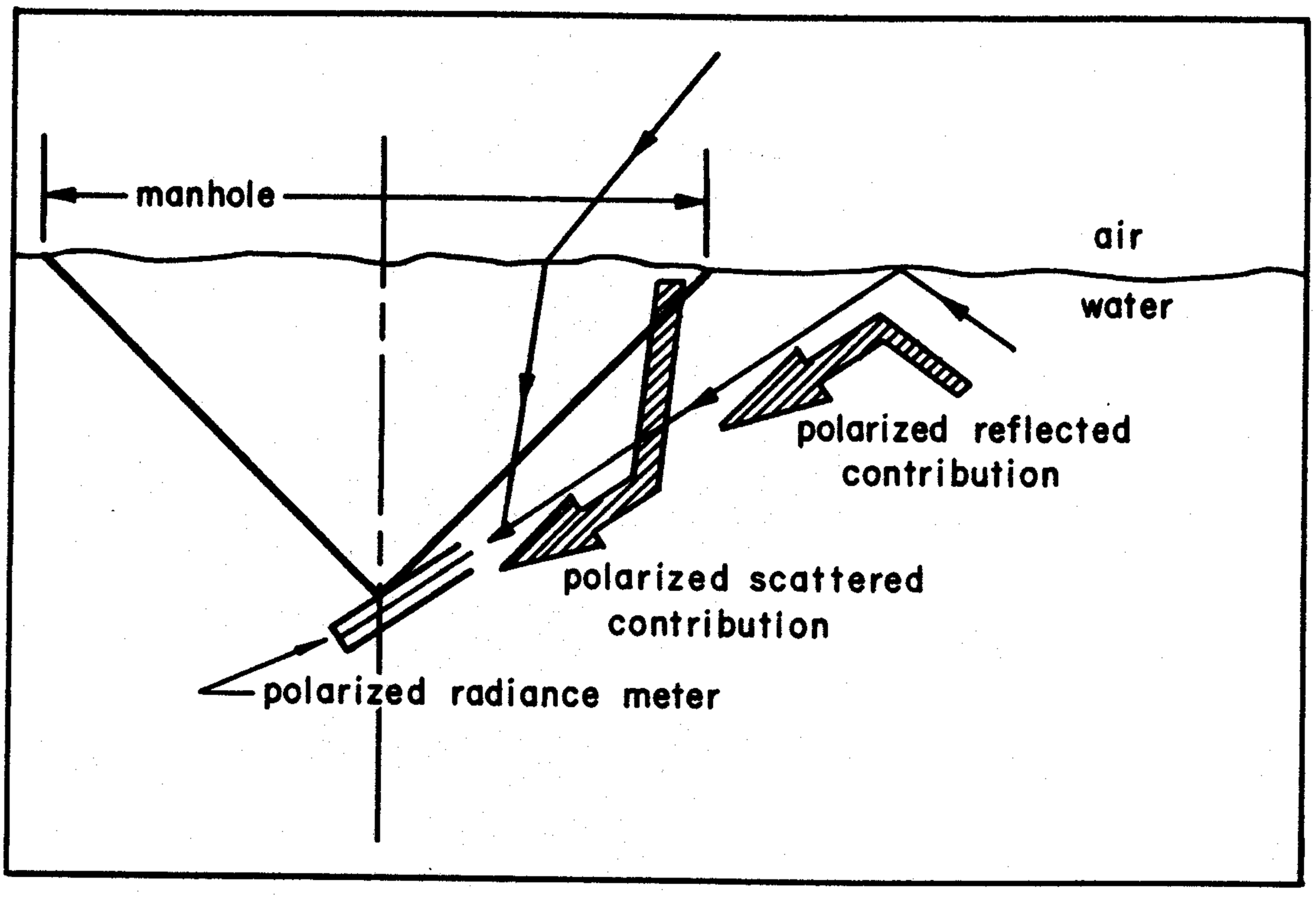

FIG. 1.36 The observed underwater polarized radiance can come from the sky via refraction through the manhole, or from the underwater domain via air-water surface reflection outside the manhole.

of the air-water surface outside the manhole (see Fig. 1.36). These two mechanisms, the scattering and reflection of underwater light, contribute the principal polarized parts to the underwater light field. On purely theoretical grounds (which need not concern us here) one would expect the scattered light to be predominantly linear, and the reflected light to be elliptical, and hence the general underwater light field to be a mixed linear-elliptical polarized field (see Sec. 2.10 and the Stokes Polarization Composition theorem).

The general features of polarized submarine light fields may be summarized, according to Ivanoff and Waterman [117], [118], as follows. In general for a fixed direction ξ the polarization $p(x,\xi)$ is greatest near the air-water surface, and diminishes rapidly with depth down to about 10-20 attenuation lengths and then settles down to an asymptotic value, which does not change with further increase of depth (this is reminiscent of the asymptotic radiance theorem described earlier; and in Sec. 4.6 the potential connections between these two ideas will be outlined). Furthermore, the limiting p value depends on the water clarity, and we would expect on theoretical grounds that it eventually be independent of surface and bottom effects provided the medium is deep enough. It is noted that, all other factors remaining fixed, polarization increases rapidly with transparency from turbid to moderately clear waters, but the increase slows down as waters become more and more transparent. In oceanic hydrosols p may vary,

e.g., from .60 at the surface to .30 as an asymptotic value. In a horizontal sweep, with low sun, the azimuth dependence of p is generally such that in directions normal to the vertical plane of the sun p is greatest, less for directly away from the sun and least of all looking toward the sun. For higher suns or for more turbid waters a horizontal sweep of the radiance tube may find little variation in p. The wavelength dependence of p is such that, with all other factors remaining fixed, p attains a minimum at the blue-green wavelengths (450 mμ)--i.e., just about where in the spectrum natural waters transmit best. This ties in with the observations cited just above about turbidity dependence of p. (Remember the proviso, "all other factors remaining fixed".) Thus both ends of the spectrum should yield higher p values, and hence more pronounced polarized fields in reddish and bluish light --of what there is to measure. The polarization of underwater light fields decreases when diffuseness of the field increases. For example, when depths are shallow, overhead cloudiness will tend to increase the diffuseness and hence decrease the polarization. Under best conditions, the elliptical component of the underwater radiance field reaches about 10% of the total radiance, and about 50% of the linear component. At very great depths the light is predominantly horizontally linearized (because the predominant flow is downward; and recall the analogy with scattered skylight).

Further details will be found in [117], [118], and also in Tyler's article [301]. A simple model for polarized light fields in the sea is developed, along with the general theory, in Sec. 4.6. Sec. 2.10 develops the essentials of the radiometry of polarized light.

Biological Sources of Submarine Light Fields

How many have ever seen the unforgettable sight of luminous bow waves of a ship plowing through nighttime tropical and semitropical waters? Many types of marine animals large and small are known to emit radiant energy when disturbed--a sort of pale cold light, obviously of chemical (quantum) rather than thermal origin. Other organisms seem to flash on and off under their own volition, deep in the sea or in nighttime waters nearer the surface.

An important study of such self-regulative radiometric-biologic phenomena was made by Kampa and Boden [133] in which detailed and careful measurements of the radiant flux output of a certain type of luminescent creatures (*Euphasia pacifica*) were made both *in situ* in the San Diego Trough, and in the laboratory. The presence of these creatures is generally noted by sonar operators because the creatures form a sonic-scattering layer in the water. By lowering a bathyphotometer (a radiant flux meter tightly encased for deep water work) down into the layer, day and night recordings of the output of the *Euphasia* were made.

It was observed that the creatures emitted flashes having a *mean* irradiance of about 1.1×10^{-4} microwatts/cm^2 throughout the day. The output was in the form of flashes

which varied in frequency as a function of time of day--greatest (42/min) during twilight when the *Euphasia* migrated upward, least (10-24/min) during midday when they were at rest in the depths, and intermediate (32/min) during the night. The color of the luminescence was blue-green, with maximum output near 478 mμ, and a secondary maximum near 520 mμ. Kampa and Boden postulate that the time dependence of the depth of the *Euphasia* scattering layer is photoregulated; that is, the creatures constantly monitor the environmental level of irradiance and according raise or lower themselves to a depth at which the total irradiance ($H(z,+) + H(z,-)$) is on the order of 10^{-4} microwatts/cm^2. All this activity transpires along with the flashing at the above-mentioned mean irradiance and frequencies. The type of flashes are temporally highly peaked and these peaks were observed to be one to two orders of magnitude greater than the total environmental irradiance (see Fig. 1.37). It appears that this is an optical means of assuring togetherness during the vertical migrations, for the eye pigment of the *Euphasia* has a greatest photosensitivity to the predominant color of its flashes.

Using the irradiance models developed in Chapter 8, it is a relatively straightforward task to describe and predict the light field generated in the sea by extensive layers of the *Euphasia* or other stratified biological sources of radiant flux. The photoregulative activities of these creatures coupled with the general food chain activities in the seas

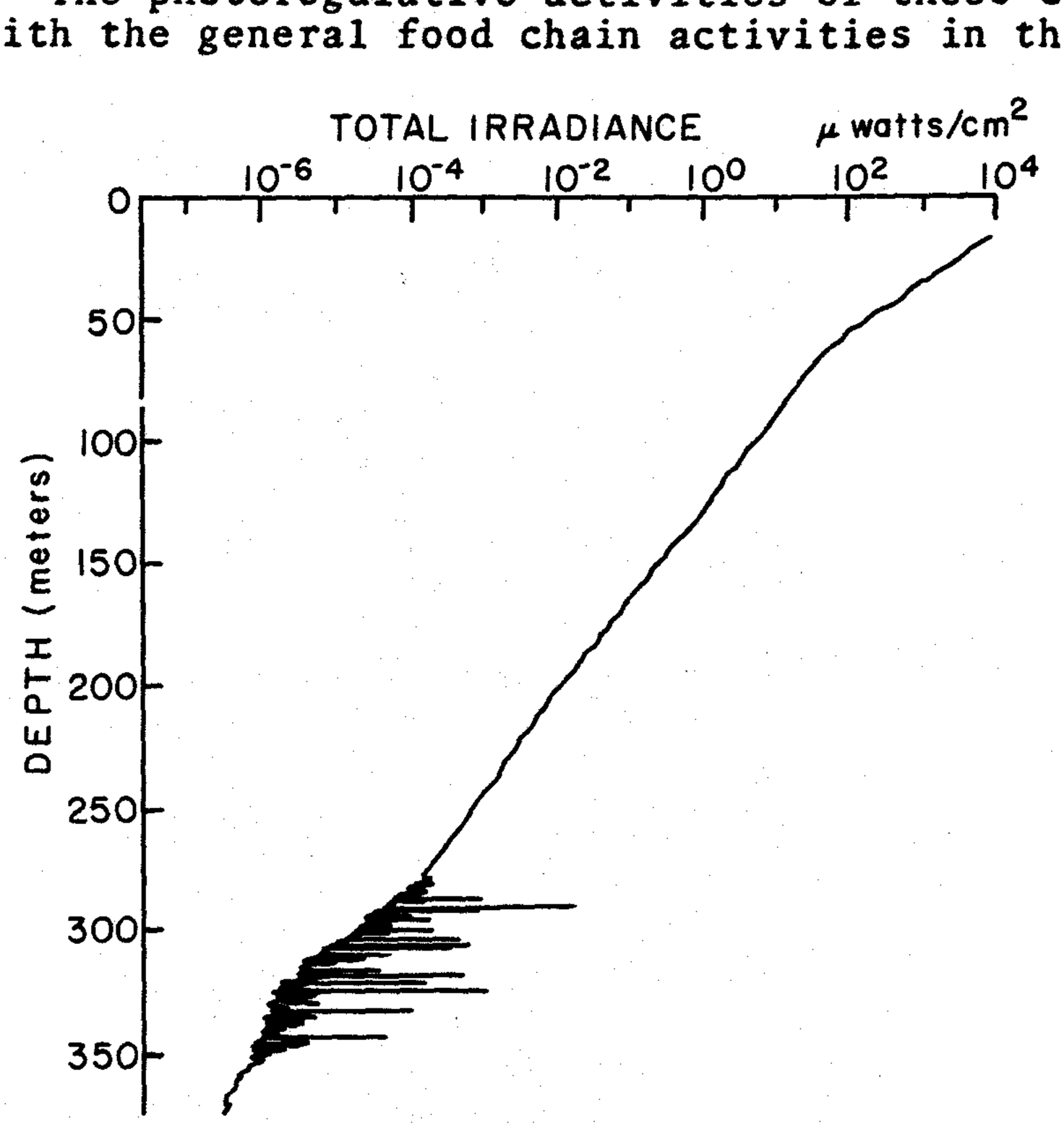

FIG. 1.37 Depth dependence of downward irradiance in which discrete flashes of light generated by *Euphasia pacifica* are evident at the depths around 300-350 meters, as observed by Kampa and Boden in the San Diego Trough, 20 February 1956. (From [133], by permission)

presents a challenging problem to hydrologic optics in the description of the dynamical interactions of plants, animals and photons in seas and lakes. We shall briefly reconsider this problem in Sec. 1.10.

<< Table of Contents << Title Page >> Next Page >>

1.3 Three Simple Models for Light Fields

How do we seek order in all that we have encountered above? How do we incorporate those few evidences of order, already glimpsed, into some greater scheme, satisfying for its accuracy, comprehensiveness, and relevance to the main stream of modern physical theory? The number of effects to be described is great, and their intricacy has a tendency to initially intimidate those who attempt a precise description: nature's ways are orderly but infinitely complex, the theorists are few and finite; therefore, each stage of theoretical knowledge inevitably rests on chosen compromises. Three such theoretical compromises are selected for study here; each is designed to describe one facet of the radiometric complex encountered in the seas and lakes of the earth: the first two describe the light fields generated by sunlight and skylight and give simple models for the radiance distributions and two-flow irradiance fields; the third describes artificial light fields set off in the water by man-made point sources and extended artificial sources of radiant flux.

The Two-Flow Model

The two-flow model of the light field pictures the radiant flux in a natural hydrosol X, free of internal sources, as divided into two streams at each depth z below the boundary: a downward stream of radiance H_- and an upward stream of irradiance H_+ (see Fig. 1.38). The primary purpose of the model is to predict H_+ and H_- at each depth z, given H_+ and H_- at the upper boundary, or more generally, given H_+ at some depth and H_- at another (possibly the same) depth. The hydrosol, therefore, is viewed by this model as a *plane-parallel medium*, i.e., an infinite region of space caught between two horizontal parallel planes, which are the *boundaries* of the medium. The physical properties of the hydrosol are described in the present model by means of two optical properties a, b; and the geometrical flow of the radiant energy is described by means of a *distribution factor* D. These three concepts are defined in detail as follows. We write:

"a" for the amount of irradiance *absorbed* from a narrow vertical beam of radiant flux of unit irradiance as it crosses a horizontal layer of unit thickness in X.

"b" for the amount of irradiance *back scattered* without change in wavelength from a given arbitrary stream of radiant flux of unit irradiance as it crosses a horizontal layer of unit thickness in X.

Finally, if h_+, h_- are the scalar irradiances associated with